5101-201
Flat-Plate
Solar Array Project

DOE/JPL-1012-69
Distribution Category UC-63b

An Investigation of the Effect of Wind Cooling on Photovoltaic Arrays

L. Wen

March 1982

Prepared for
U.S. Department of Energy
Through an Agreement with
National Aeronautics and Space Administration
by
Jet Propulsion Laboratory
California Institute of Technology
Pasadena, California

(JPL PUBLICATION 82-28)

5101-201
Flat-Plate
Solar Array Project

DOE/JPL-1012-69
Distribution Category UC-63b

An Investigation of the Effect of Wind Cooling on Photovoltaic Arrays

L. Wen

March 1982

Prepared for
U.S. Department of Energy
Through an Agreement with
National Aeronautics and Space Administration
by
Jet Propulsion Laboratory
California Institute of Technology
Pasadena, California

(JPL PUBLICATION 82-28)

Prepared by the Jet Propulsion Laboratory, California Institute of Technology, for the U.S. Department of Energy through an agreement with the National Aeronautics and Space Administration.

The JPL Flat-Plate Solar Array Project is sponsored by the U.S. Department of Energy and is part of the Photovoltaic Energy Systems Program to initiate a major effort toward the development of cost-competitive solar arrays.

ABSTRACT

Convective cooling of photovoltaic modules is investigated for different wind conditions, including steady-state controlled testing in a solar simulator and natural test environments in a field. Analytical thermal models of different module designs were used to correlate experimental data. The results obtained in the controlled environment confirm the applicability of existing heat-transfer correlations. The result of long-term field testing at the Jet Propulsion Laboratory test site is not conclusive because wind conditions were measured at different heights than that of the modules. Nevertheless, reasonable agreement can be obtained by applying a power-law wind profile.

ACKNOWLEDGMENTS

The author wishes to thank, for their assistance in this investigation, J. Griffith, for discussion of the controlled wind testing of arrays in solar chamber; R. Weaver, for field-test data; and D. Stong, for data reduction.

This publication reports on work done under NASA Task RD-152, Amendment 66, DOE/NASA IAA No. DE-AI01-76ET20356.

GLOSSARY

ABBREVIATIONS AND ACRONYMS

AM	Air mass
ASEC	Applied Solar Electric Corp.
DOE	U.S. Department of Energy
FSA	Flat-Plate Solar Array (Project)
JPL	Jet Propulsion Laboratory
NASA	National Aeronautics and Space Administration
NOCT	Nominal Operating Cell Temperature
NTE	Nominal Terrestrial Environment
PV	Photovoltaic(s)

DEFINITION OF SYMBOLS

Symbols	Description	Units
A	area	m^2
C	unit conductance	$W/m^2 \cdot {}^oC$
Cp	specific heat	kWh/kg
g	load factor	
H	forced-convection coefficient	$W/m^2 \cdot {}^oC$
h	free-convection coefficient	$W/m^2 \cdot {}^oC$
k	thermal conductivity	$W/cm \cdot {}^oC$
L	characteristic thickness	cm
M	mass	kg
m	sensitivity constant	$^oC \cdot cm^2/mW$
P	electric-power conversion	W
Q	thermal energy	mWh
S	insolation	mW/cm^2
T	temperature	c, K
t	time	min., h
U	measured wind speed	m/s
V	effective wind speed	m/s
α	solar absorptance	
ϵ	emittance	
ξ	conversion efficiency	
η	relative coefficient	
ψ	module tilt angle deg	
ϕ	weighting function	
σ	Stefan-Boltzmann constant	$mW/cm^2 \cdot {}^oK^4$
β	exponent coefficient	

CONTENTS

Figures

Tables

SECTION I

INTRODUCTION

The Jet Propulsion Laboratory's (JPL) Flat-Plate Solar Array Project (FSA) has sought to define design requirements, design analysis and test methods, and design approaches for flat-plate arrays and modules, to define means of reducing the cost and improving the utility and reliability of photovoltaic (PV) modules for terrestrial applications. This report presents the results of a study carried out as part of the FSA Engineering Sciences Area to improve the understanding of field wind conditions on module and array performance.

The performance of solar arrays depends upon two key parameters: incident irradiance (level and spectral composition), and the junction temperature of the PV device. At present, the most widely accepted insolation reference condition is a total irradiance of 100 mW/cm^2 at air mass (AM) 1.5 spectrum. Reference solar-cell efficiency, ξ_o, is referred to the value rated at the reference insolation and a cell temperature of 28°C (References 1 and 2). As expressed in Equation (1), the effective PV conversion efficiency, ξ, is the reference efficiency modified by two coefficients: a relative temperature coefficient, η_T, and an irradiance coefficient, η_S.

$$\xi = \xi_o \cdot \eta_T \cdot \eta_S \tag{1}$$

For silicon devices, the reference cell efficiency, ξ_o, at 28°C and 100 mW/cm^2, ranges from 9 to 16%. The relative temperature coefficient, η_T, expressed in Equation (2) shows a 0.5% reduction per degree Celsius increase in cell temperature, T_{cell}.

$$\eta_T = 1.1456 - 0.0052\, T_{cell} \tag{2}$$

The relative irradiance coefficient, η_S, can be approximated by Equation (3) in terms of the effective insolation, S, in mW/cm^2.

$$\eta_S = \left[0.143 \log_{10}\left(\frac{S}{140}\right)\right] + 1.02 \tag{3}$$

For PV arrays, the cell operating temperature is a complex function of the module thermal design and the site's environmental conditions, which include the irradiance level, ambient temperature, and wind conditions. To provide a relative-performance basis for different module designs, a reference characterization test procedure was proposed to measure the Nominal Operating Cell Temperature (NOCT) in a defined Nominal Terrestrial Environment (NTE) (Reference 3). NOCT is defined as the cell temperature of a module at a specified insolation (80 mW/cm^2), 20°C ambient temperature, 1 m/s wind speed (not east or west wind), and open-circuited. The approach is based upon

the observation that the cell-ambient temperature difference, $T_{cell} - T_{amb}$, of a typical solar array is largely independent of ambient temperature and is essentially linearly proportional to the insolation level, S.

Accurate prediction of solar-array performance is difficult because of variations in solar irradiance, ambient temperature, and wind conditions. Current practices have been based upon recordings of weather data to assess long-term electric-power production of a PV module. For most weather-data records, such as the SOLMET formatted tapes (Reference 4), the recordings are made hourly and the measurements represent the instantaneous values observed a few minutes before each hour.

There are two different approaches in assessing long-term PV power production. One of them does not account for the variable wind effect of different wind velocities on module cooling, but includes a fixed term based on typical mild-wind field conditions. Equation (4) is a sample expression for a representative PV module. The sensitivity coefficient, m, was evaluated at $0.3^{o}C \cdot cm^2/mW$, based upon long-term field-test data (References 1 and 2) with an average wind of 1 m/s.

$$T_{cell} = T_{amb} + m \cdot S \qquad (4)$$

In this approach the performance prediction is based upon experimental observations, where a typical long-term wind-cooling effect is automatically included in the sensitivity coefficient, m. The prediction has been found to be reliable for solar-array sites with mild-wind conditions.

The other approach in assessing PV power production relies upon explicit analytical simulation of the module thermal response using weather-tape wind data. The wind effect on module temperature is computed according to established heat-transfer correlations such as those shown in Reference 5.

Theoretically, the assessments resulting from these two different approaches should be compatible on a long-term basis. However, in real practice, some apparent discrepancies have been experienced. It is the primary objective of this investigation to understand these disagreements.

SECTION II

FUNDAMENTAL HEAT-TRANSFER CORRELATIONS

The thermal behavior of a flat-plate PV module can be described by the energy-balance relationship expressed in Equation (5). The amount of solar energy absorbed by a module should be equal to the sum of the following quantities: convective and radiative heat losses to the ambient environment, power converted into electricity, and change in thermal energy content.

$$A\alpha S = Q_{\substack{free \\ conv}} + Q_{wind} + Q_{rad} + P + MC_P \frac{dT}{dt} \qquad (5)$$

where

A = effective module area

α = effective solar absorptance

S = insolation

$Q_{\substack{free \\ conv}}$ = free-convection heat loss

Q_{wind} = heat loss caused by wind cooling

Q_{rad} = radiative heat loss

P = power conversion to electricity

MC_p = thermal capacitances of module

T = effective module temperature

t = time

Equation (5) treats the entire module as a lumped mass unit. However, because all PV modules are composites of encapsulants, cells, intercell spaces, substrates, and mounting structures, complex nodal models can also be established for each component of the module. For the purpose of simplicity, the single-node model is often used and all properties take the weighted average values of individual components.

A. SOLAR ENERGY ABSORPTION

The active surface of a PV module consists of composite layers of cell ensembles, encapsulants and interconnectors. Typical module designs have 60 to 90% active cell area, whose measured solar absorptivities are in the

0.85 to 0.9 range. The solar absorptivity of intercell spaces may vary significantly depending upon surface conditions and coating applications. The effective solar absorptance is then a weighted average of the two components.

B. RADIATIVE HEAT LOSS

Radiative heat transfer between a PV module and its environment may be affected by the ground temperature and view factors. However, for most flat-plate module applications, one may consider that the front-surface views only the sky while the back surface is either insulated (roof mounted) or has a unit view factor to the ground.

In a field arrangement, most of the effective ground area is in shadow. Ambient air temperature may be used as a good approximation for the effective ground temperature. Equation (6) gives a close approximation for the module radiative heat loss.

$$Q_{rad} = \epsilon_f A\sigma(T_f^4 - T_{sky}^4) + \epsilon_g \epsilon_b A\sigma(T_b^4 - T_{amb}^4) \qquad (6)$$

where

ϵ_f, ϵ_b = surface emittance of the front and back surface

T_f, T_b = front and back surface temperatures

ϵ_g = ground emittance and takes a nominal value of 0.8

T_{sky} = sky temperature

σ = Stefan-Boltzmann constant, 0.56699×10^{-8} mW/cm^2.°K^4

All temperatures in Equation (6) are expressed in the absolute scale (i.e., Kelvin). T_{sky} can be related to T_{cell} by the relationship established based upon NASA measurement (Reference 6) as shown in Equation (7).

$$T_{sky} = 0.914\ T_{amb}\ (^oK) \qquad (7)$$

C. POWER CONVERSION

Total power extraction from a PV module is governed by the conversion efficiency and the load condition as shown in Equation (8).

$$P = S \cdot A_c \cdot \xi \cdot g \qquad (8)$$

where

A_c = active cell area

g = load factor

The load factor, g, specifies the electric load condition, $0 \leq g \leq 1$; $g = 1$ for maximum power tracking, and $g = 0$ for no-load condition.

D. THERMAL INERTIA

The thermal inertia of a PV module is determined by the module design. Table 2-1 lists the thermal inertia, along with other relevant thermal-optical properties, for four baseline PV module designs that are used throughout the

Table 2-1. Representative Photovoltaic Module Specifications

	Module Design A (Sensor Technology)	Module Design B (Spectrolab)	Module Design C (Solarex)	Module Design D (Solar Power)
No. of Cells	25	20	18	22
Cell Diameter, cm	5.08	5.4	7.62	8.64
Cell Area/ Module Area, %	53.7	57	69.75	68.28
Module Dimensions, cm	16.5 x 57.2	12.4 x 64.8	24.4 x 48.2	33.0 x 57.15
Substrate	aluminum extrusion 12 short fins	aluminum extrusion single fin	G10 board	G10 board
Solar Absorptance	0.66	0.688	0.76	0.776
Front-Surface Emittance	0.91	0.86	0.88	0.88
Back-Surface Emittance	0.85	0.86	0.98	0.88
Thermal Inertia Wh/^{o}C	0.261	0.532	0.288	0.851
Specific Thermal Inertia Wh/^{o}C$\cdot$m^2	2.766	6.626	2.447	6.43

present investigation. The following module designs are the Block I procurement for FSA in 1976:

Module design A: Sensor Technology
B: Spectrolab
C: Solarex
D: Solar Power

Module designs A and C have similar specific thermal inertia around 2.5 $Wh/^{o}C \cdot m^2$. A complete shading of the module from solar irradiation for 1 min would result in a temperature change of about 5°C. For module designs B and D the corresponding temperature change would be less than 2.5°C, because of their larger thermal inertia.

E. FREE CONVECTION

Both front and back surfaces of open-frame-mounted flat-plate PV modules are exposed to ambient air. Free-convective heat transfer can be calculated by Equation (9).

$$Q_{\substack{free \\ conv}} = (h_f + h_b)\,\Delta T \tag{9}$$

where h_f and h_b are the coefficients of heat transfer for the front and back surfaces, respectively.

Approximations for the turbulent free-convective heat-transfer coefficients for the front and back surfaces tilted upward at an angle ψ are shown in Equations (10) and (11), respectively (Reference 7).

$$h_f = 1.52\,(\Delta T \cos \psi)^{1/3} \tag{10}$$

$$h_b = 1.31\,(\Delta T \sin \psi)^{1/3} \tag{11}$$

In each of these equations, the coefficient of heat transfer is expressed in $W/m^2 \cdot {}^{o}C$; ΔT is the temperature difference between the surface and the local air temperature. The relationships are for a ψ angle less than 70 deg.

F. FORCED CONVECTION CAUSED BY WIND

Forced convection of wind over a flat-plate PV module involves a large number of variables such as wind speed, wind direction, time-dependent fluctuations, module surface characteristics, tilt angles, and wind interference from terrain and structures. The general correlation is complex. However, a special case of parallel flow has been well investigated (References 8, 9, 10). For steady-state airflow over a parallel plate, the following simple formulae were found to give good correlations to experimental measurements:

$$H = 3.8\ V_{//} \quad ;\ V_{//} \leq 5\ m/s$$
$$H = 7.17\ V_{//}^{0.78};\ V_{//} > 5\ m/s \qquad (12)$$

where

H = forced-convective coefficient of heat transfer in $W/m^2 \cdot {}^oC$

$V_{//}$ = free-stream wind velocity parallel to the module, measured near the surface, in m/s

This correlation has also been checked in a series of thermal tests performed on a 1.2 x 1.2-m array made up of painted (Catalac flat black; $\alpha \approx 0.96, \epsilon \approx 0.87$) surfaces. The array was tilted 34 deg; the back surface was insulated. Air was moved across the front surface by a fan. Thermocouples were installed to monitor plate temperatures, ambient temperature, and the air-gap temperature behind the back surface. Temperature readings and incident solar flux were recorded at 5-min intervals. A thermal network model was constructed and a transient analysis was made, based upon the recorded boundary conditions.

A model correction technique was applied sequentially, corresponding to each data set, to assess the value of total convective heat-transfer coefficient. The estimated heat-transfer coefficient includes both free- and forced-convection components. Values for the forced-convection coefficient, H, were calculated by subtracting the free-convection components from the total values.

It should be noted that during the test period some wind fluctuation was observed, as fan-induced air movement was affected by natural wind conditions at the test site. Figure 2-1 shows the test data plotted against parallel wind speed, which was integrated over every 5 min period. The results correlate well with the simple relationship shown in Equation (12).

Natural wind conditions are generally much more complicated than the air movement generated under laboratory conditions. Figure 2-2 illustrates a set of representative wind speed and direction records. From a practical point of view, the instantaneous effect would be too complex to handle.

In an earlier study (Reference 10), average mean wind speed, $\bar{V}$, was used to characterize the wind condition. The effect of wind direction was considered to be averaged. The effective wind speed takes the integrated average:

$$\bar{V} = \int_{t_1}^{t_1+\Delta t} V(t) \cdot dt \qquad (13)$$

where

V(t) = instantaneous wind speed at time near the module

Δt = time duration for integration

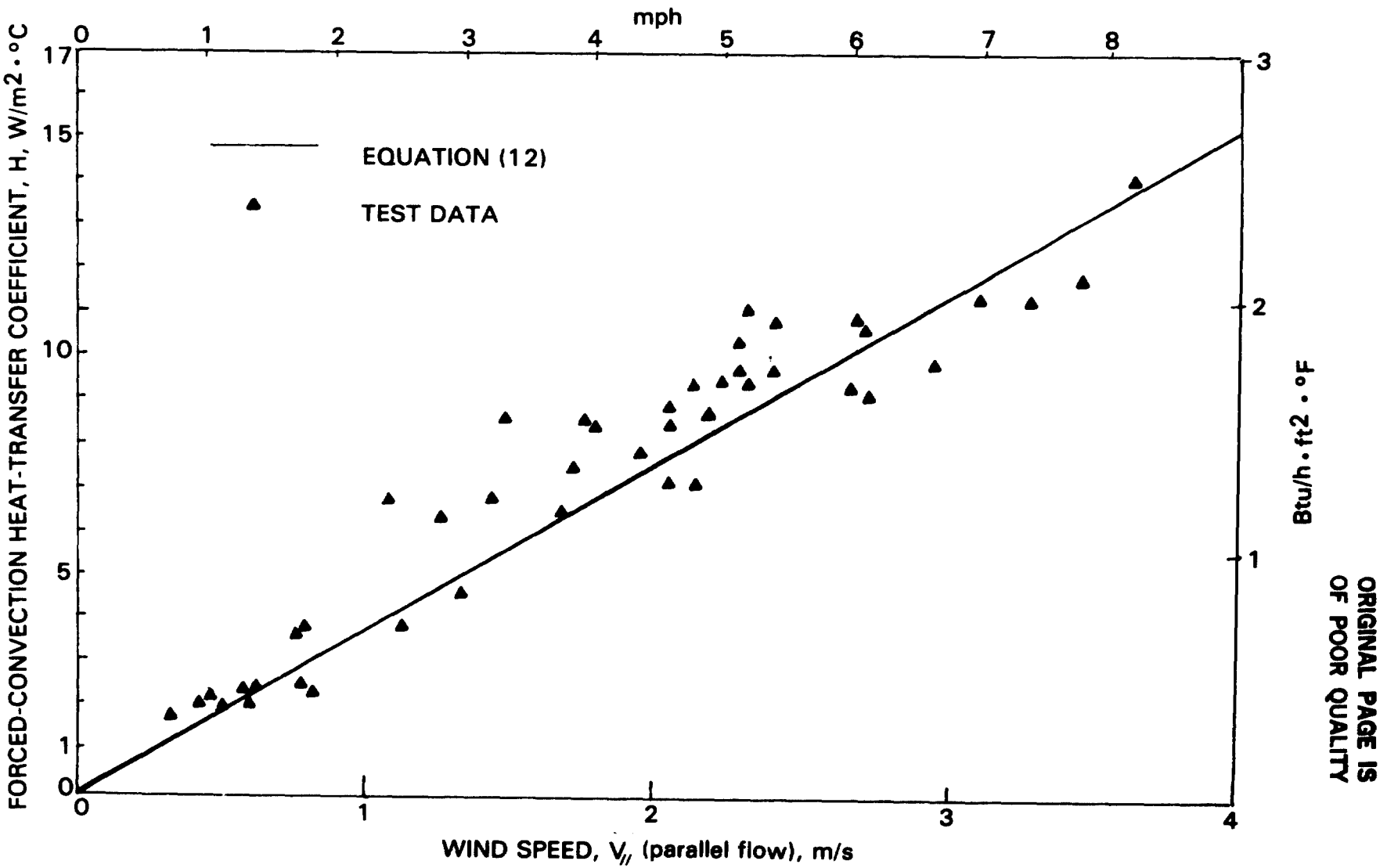

Figure 2-1. Forced-Convection Heat-Transfer Coefficient for Parallel Flow

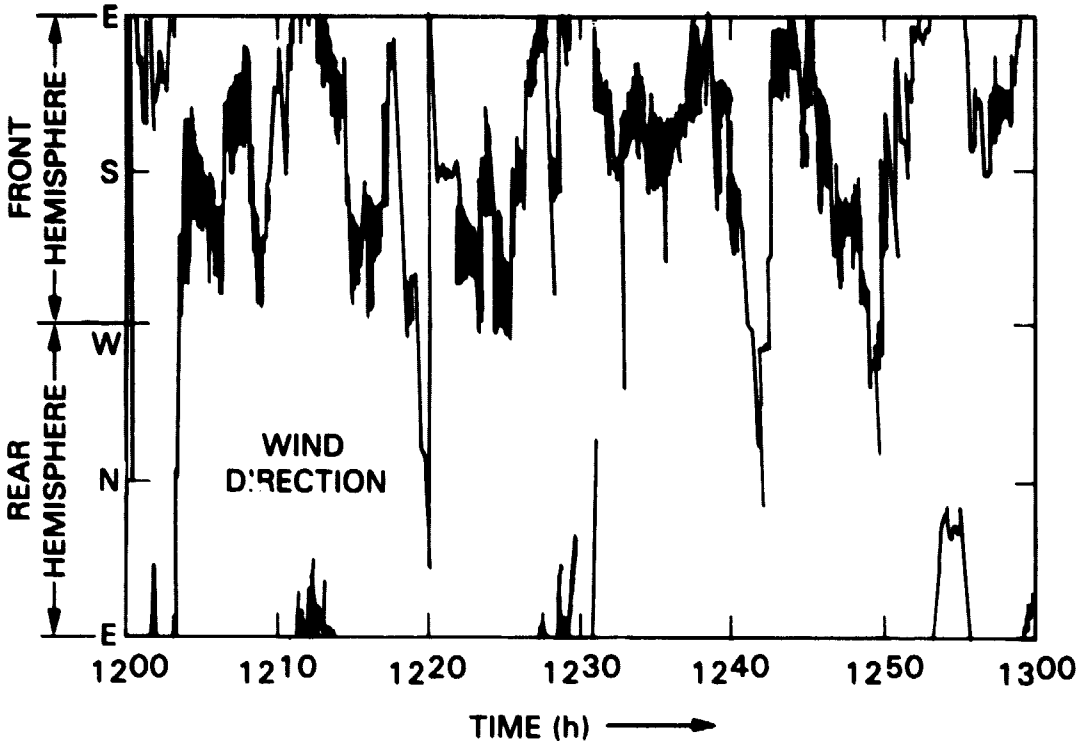

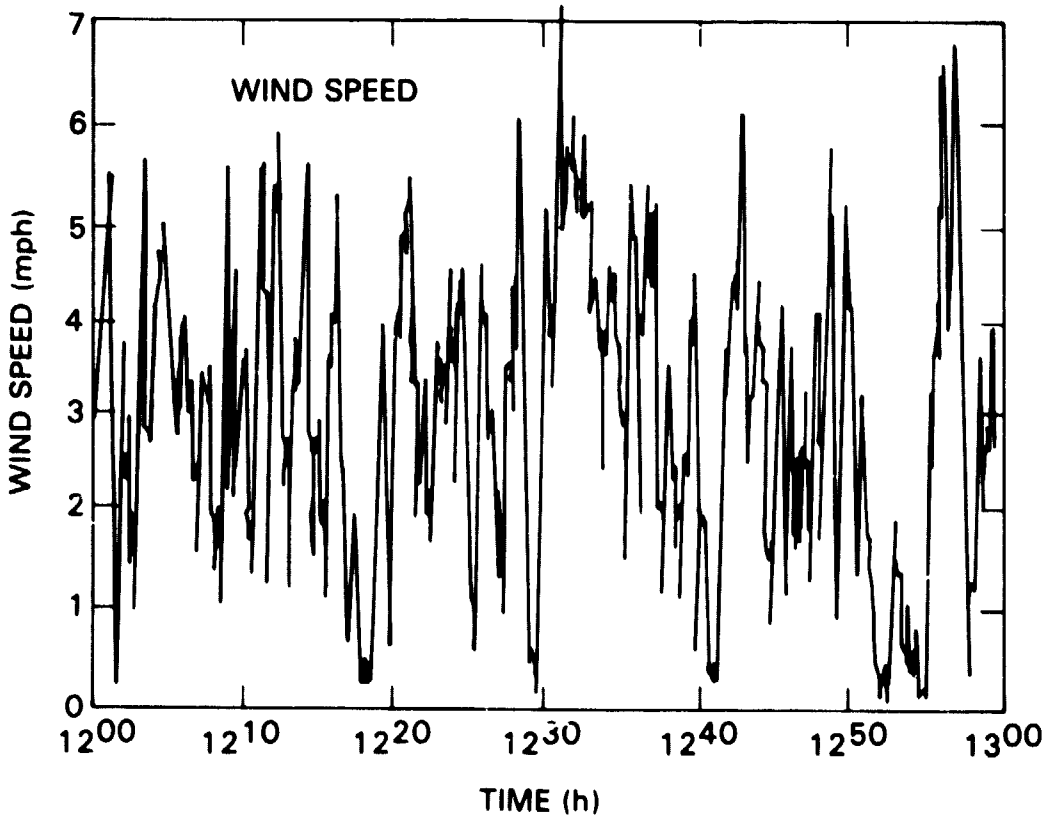

Figure 2-2. Typical Wind Conditions at JPL Field-Test Site

The values of the average wind speed were correlated to experimental measurements in PV module thermal testing. A transient thermal model correction technique using the Wiener-Kalman filtering scheme was applied to evaluate the forced-convection coefficient. The result is shown in Equation (14).

$$\bar{H} = 2.59\ \bar{V} \tag{14}$$

where

$\bar{H}$ = effective wind convection coefficient for both the front and back surfaces, $W/m^2 \cdot {}^{o}C$.

SECTION III

EXPERIMENTAL OBSERVATIONS

A. LONG-TERM FIELD TEST AT JPL

The principal photovoltaic field-test site for FSA is located at JPL. The site has 33 test stands; each can accommodate two 1.2 x 1.2-m arrays. Data acquisition includes weather data and module performance records. Weather data have been recorded at intervals, with high-frequency sampling around the time module performance data were taken. These weather data include pyranometer reading, wind speed, wind direction and ambient air temperature. Module performance data were scanned once each day (approximately 3 min to scan through a total of 226 modules). Recorded data include module I-V characteristics, peak powers, and module temperatures.

Tests began in early 1977 and the test items were dismantled in August 1981. The modules were tilted four times each year to adjust for solar declination angle changes. The tilt angle varied from 15 deg (June, July, August) to 34 deg (September, October, November, March, April, May) and 55 deg (December, January, February). A detailed description of the field-test operation is contained in Reference 11.

In the present investigation, four representative modules (Nos. 27, 70, 122, 131) were selected. Experimental data were retrieved from the period of April 1978 to July 1981. The records were first screened to eliminate obvious errors, including negative wind speed and wind speed exceeding 150 mph. Days with strong insolation variations were also excluded. The accepted data base consisted of 288 randomly selected sets of daily data. Wind condition was recorded at a height of 6 m from the ground. Mean measured wind speed was defined as the average of 12 recorded instantaneous values near the time of module temperature measurements. The data base also included records of ambient temperature and insolation variation in a period of 30 min ending at the time of module temperature measurements.

Figures 3-1 through 3-4 show the raw test data of module temperatures above the ambient, $T_{cell} - T_{amb}$, plotted against the instantaneous insolation level, S. The data fit the linear Equation (4) reasonably well. The mean sensitivity constant, $\bar{m}$, and the corresponding standard deviation are evaluated in Table 3-1.

B. CONTROLLED TESTING IN A SOLAR SIMULATOR

An experimental investigation of wind effect on PV modules was conducted in the JPL 25-ft solar simulator. A 10-hp blower with a diffuser was used to provide a uniform airflow. The test item was a PV module design by Applied Solar Energy Corporation (ASEC) (Reference 12). The module was mounted on a pedestal that could be tilted and rotated to simulate different configurations and wind directions. The pedestal was tilted toward the south, referred to as 180 deg with east at 90 deg. Wind speed was measured over the module surface by a 6000-P Alnor velometer. The results are shown in Figure 3-5 as reproduced from Reference 14.

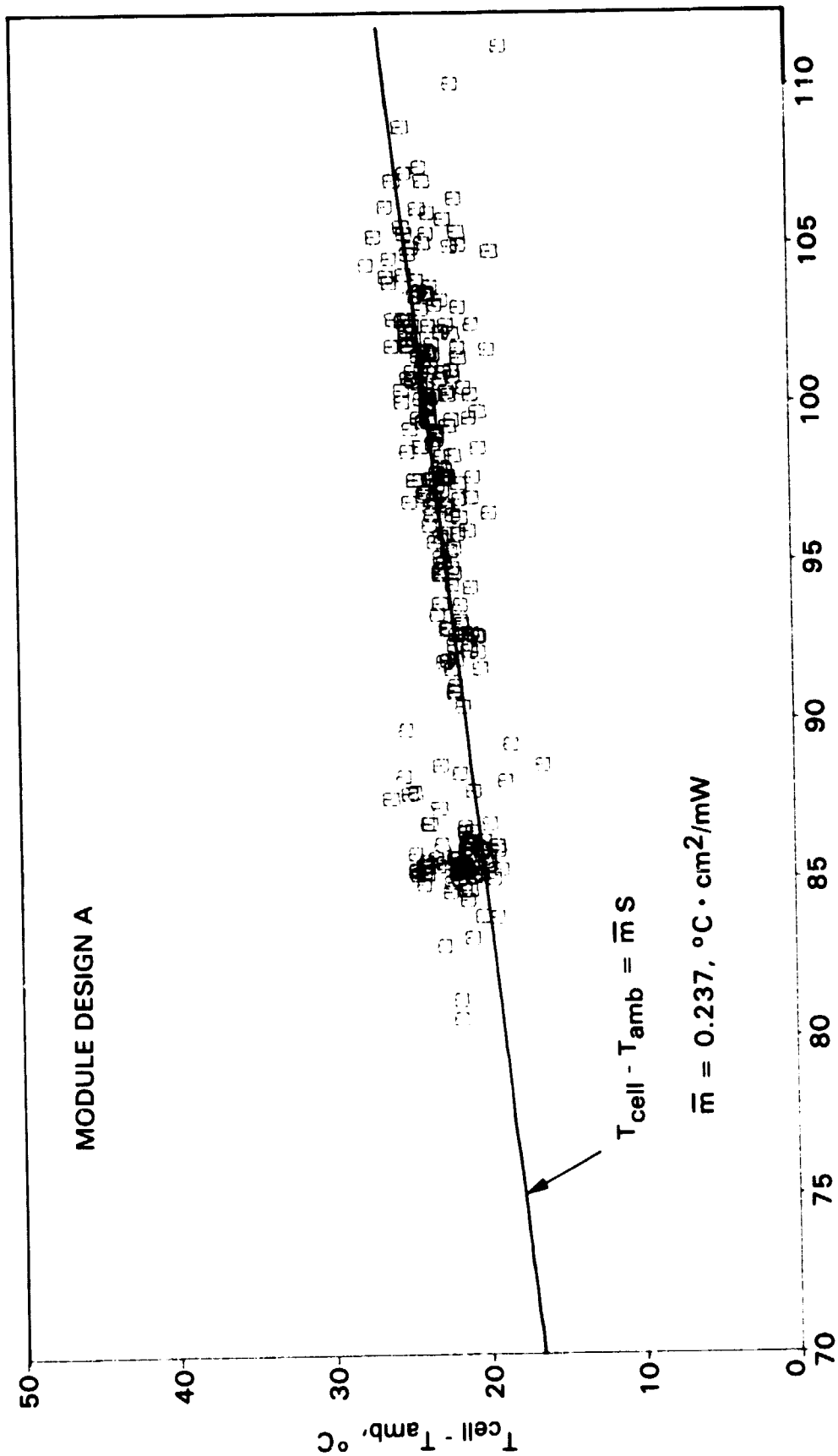

Figure 3-1. ΔT versus Insolation for Sensor Technology Block I Module

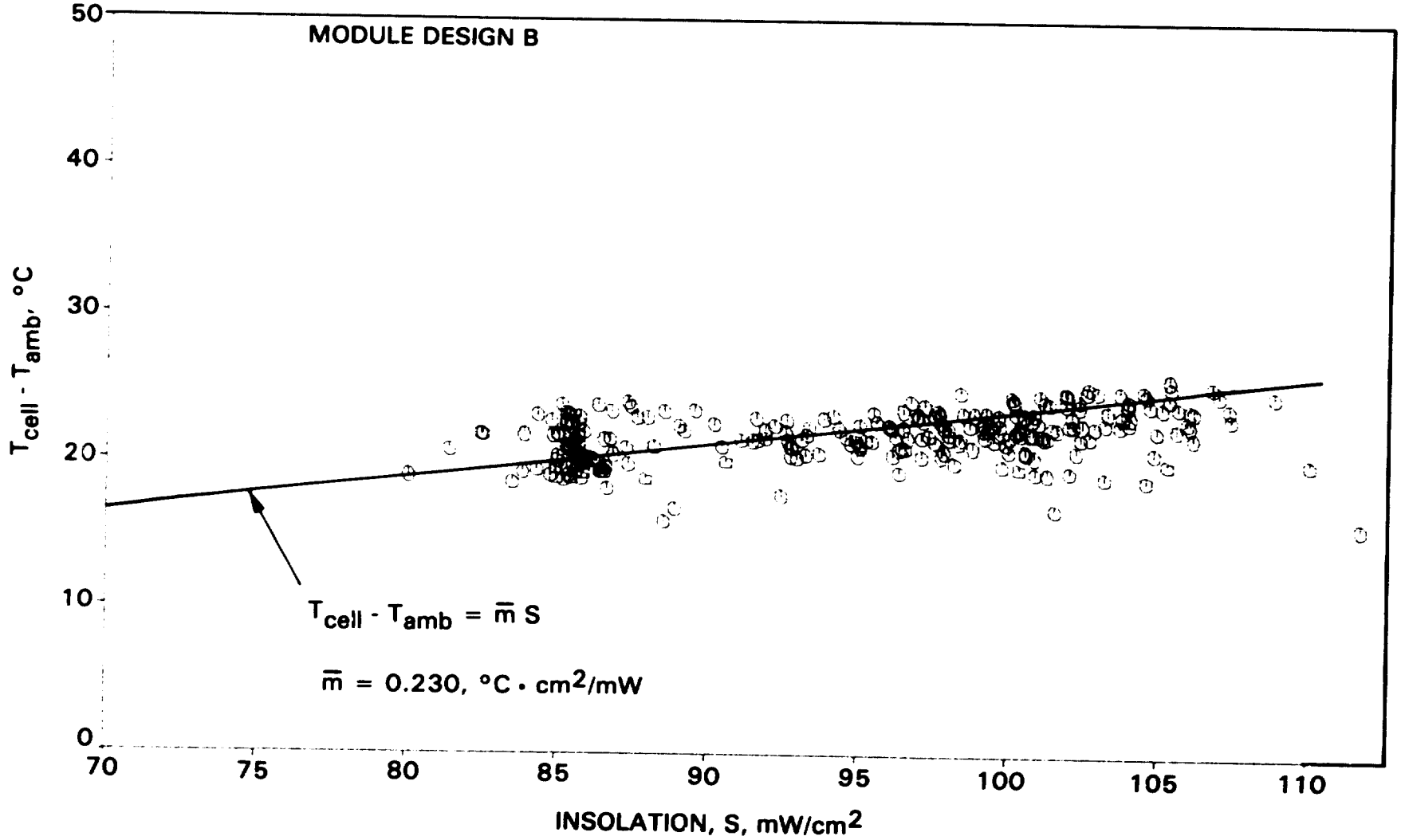

Figure 3-2. ΔT versus Insolation for Spectrolab Block I Module

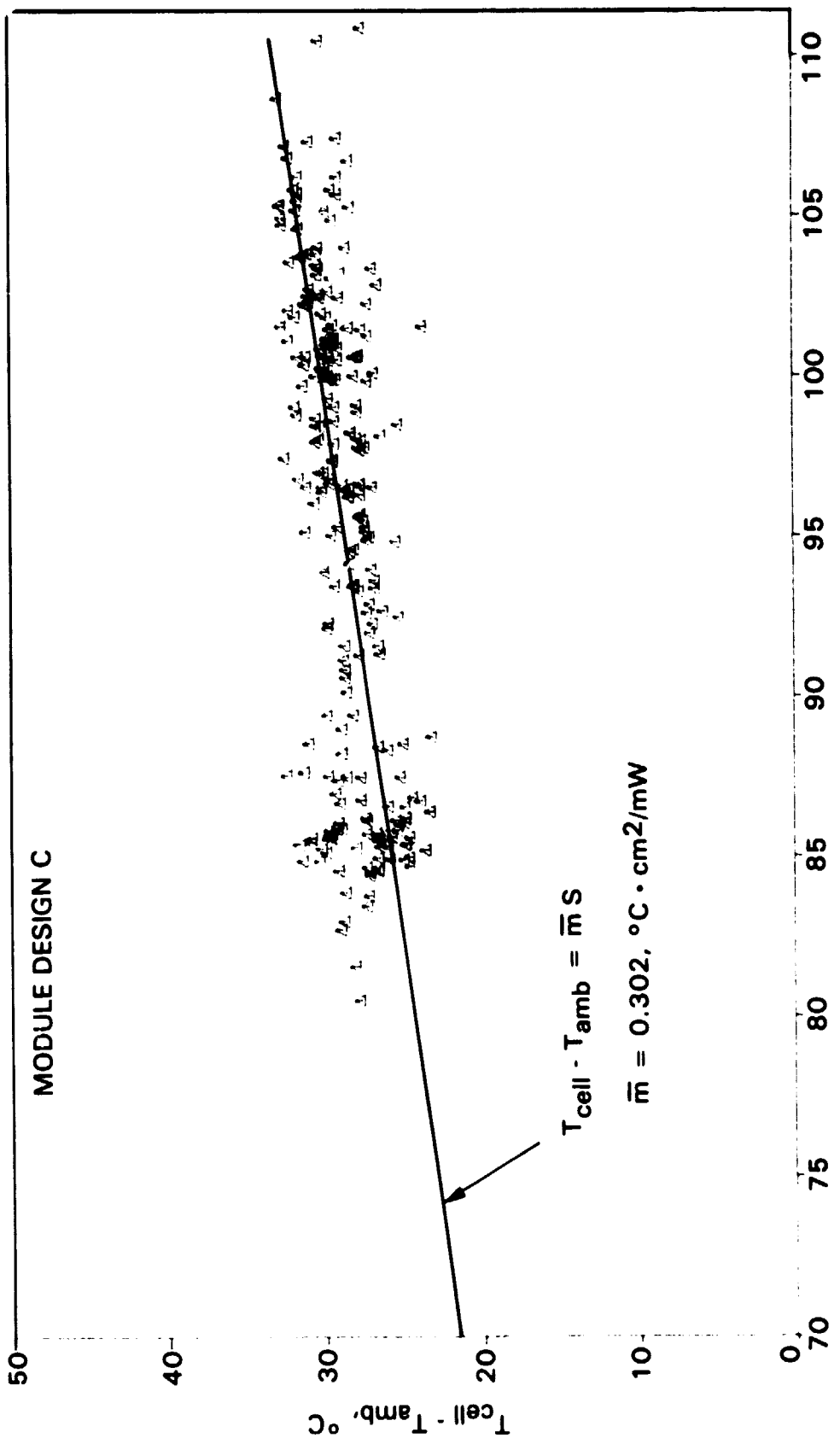

Figure 3-3. ΔT versus Insolation for Solarex Block I Module

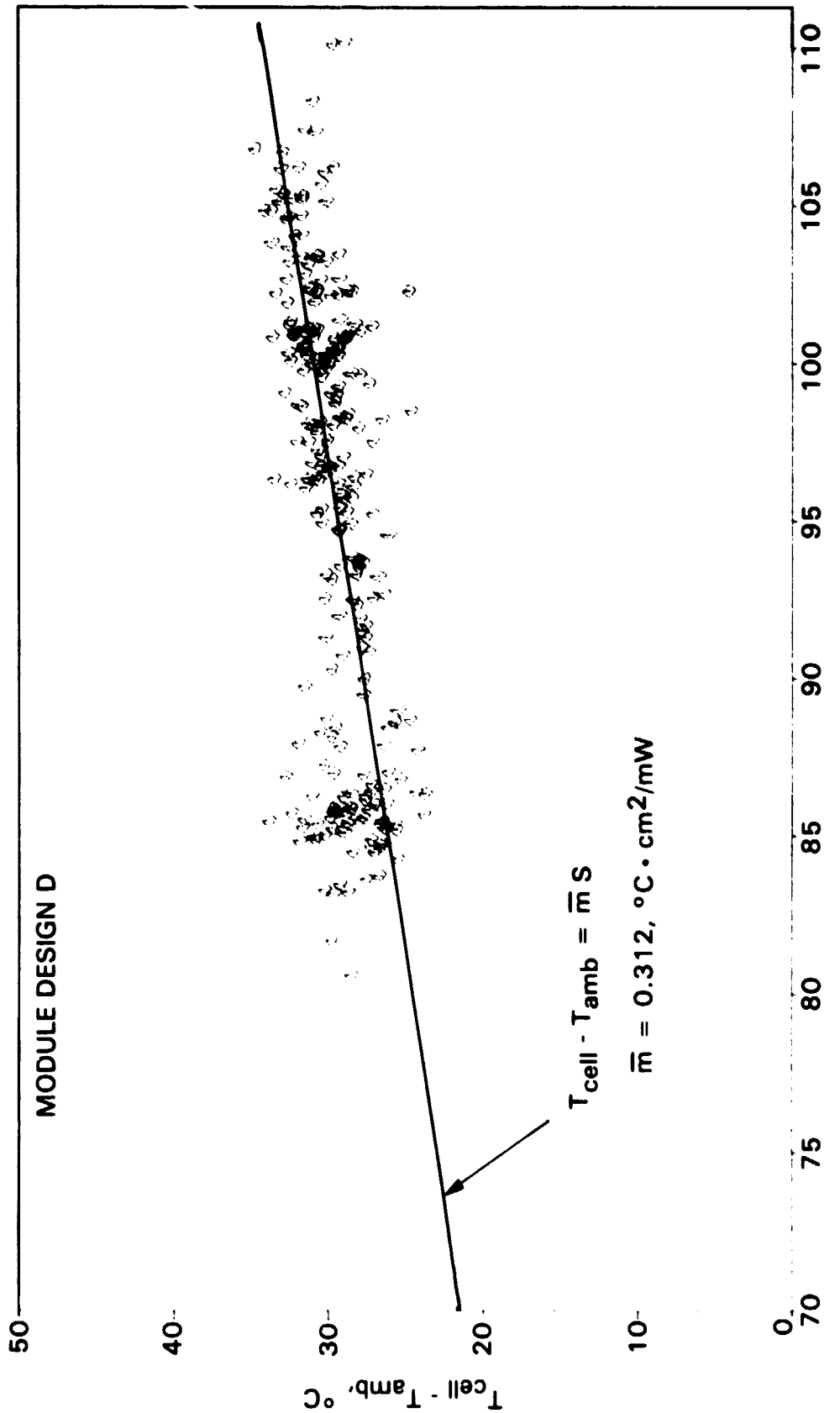

Figure 3-4. ΔT versus Insolation for Solar Power Block I Module

Table 3-1. Sensitivity Coefficient Based on Long-Term Test Data

Module Design	Manufacturer	m, $^{o}C \cdot mW/cm^2$	Standard Deviation
A	Sensor Technology	0.237	0.0198
B	Spectrolab	0.230	0.0196
C	Solarex	0.302	0.0228
D	Solar Power	0.312	0.0234

C. DISCUSSION

Results shown in Figure 3-5 indicate that cell temperature is very sensitive to wind speed, and moderately so to wind direction and ambient temperature. Cell-temperature deviations of up to 20°C, caused by a change in wind speed from 1 to 3 m/s have been observed. This corresponds to about 10% increase in electric-power production.

On the other hand, the long-term field-test data shown in Figures 3-6 through 3-9 display different characteristics. Linear regression analyses of the data indicate a very weak sensitivity to change in wind speed. This seems to support the assumption expressed by Equation (4) that cell temperature rise is dominated by insolation level only. The fact that the standard deviations in the slope constants of four modules tested are all less than 8.5% of the mean value, m, suggests that Equation (4) should be able to predict long-term energy production within 2%, at least for the JPL test site.

It should be pointed out that the conditions and measurements of these two observations were quite different and may contribute significantly to the apparent discrepancy. The data obtained from the control testing in the simulator were in steady-state conditions, while the long-term field-test data consisted of instantaneous readings.

More significantly, wind measurements in the chamber were made near the module. In the field experiments, wind speed was measured at a post 6 m above the ground. Wind profile varies significantly with height as well as with local topography. Macroscale turbulent fluctuations occur in periods of seconds (Reference 14). However, instantaneous wind oscillations are too complex to be analyzed and the wind speed reported in Figures 3-6 through 3-9 are the average value of 12 instantaneous readings recorded within 30 min of the experiment time. It was understood that such an average wind speed may not be representative of the wind condition at the time. Nevertheless, it was considered to be more realistic than using a single instantaneous reading.

Because wind speed is influenced by drag forces at the ground surface, the variation of wind speed with altitude is strongly affected by terrain

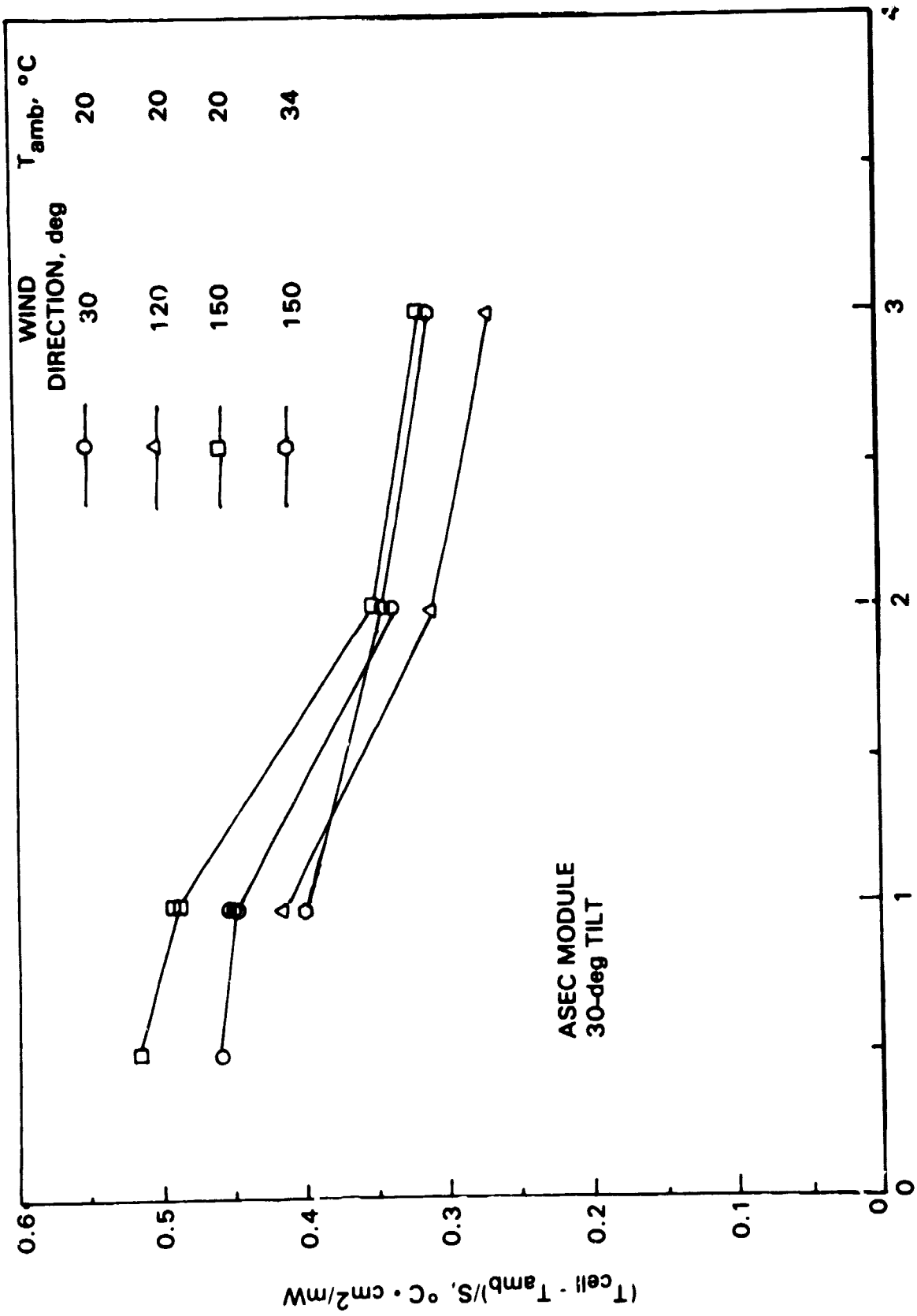

Figure 3-5. Effect of Wind Speed on Cell-Temperature Rise (Based on Controlled Test Data)

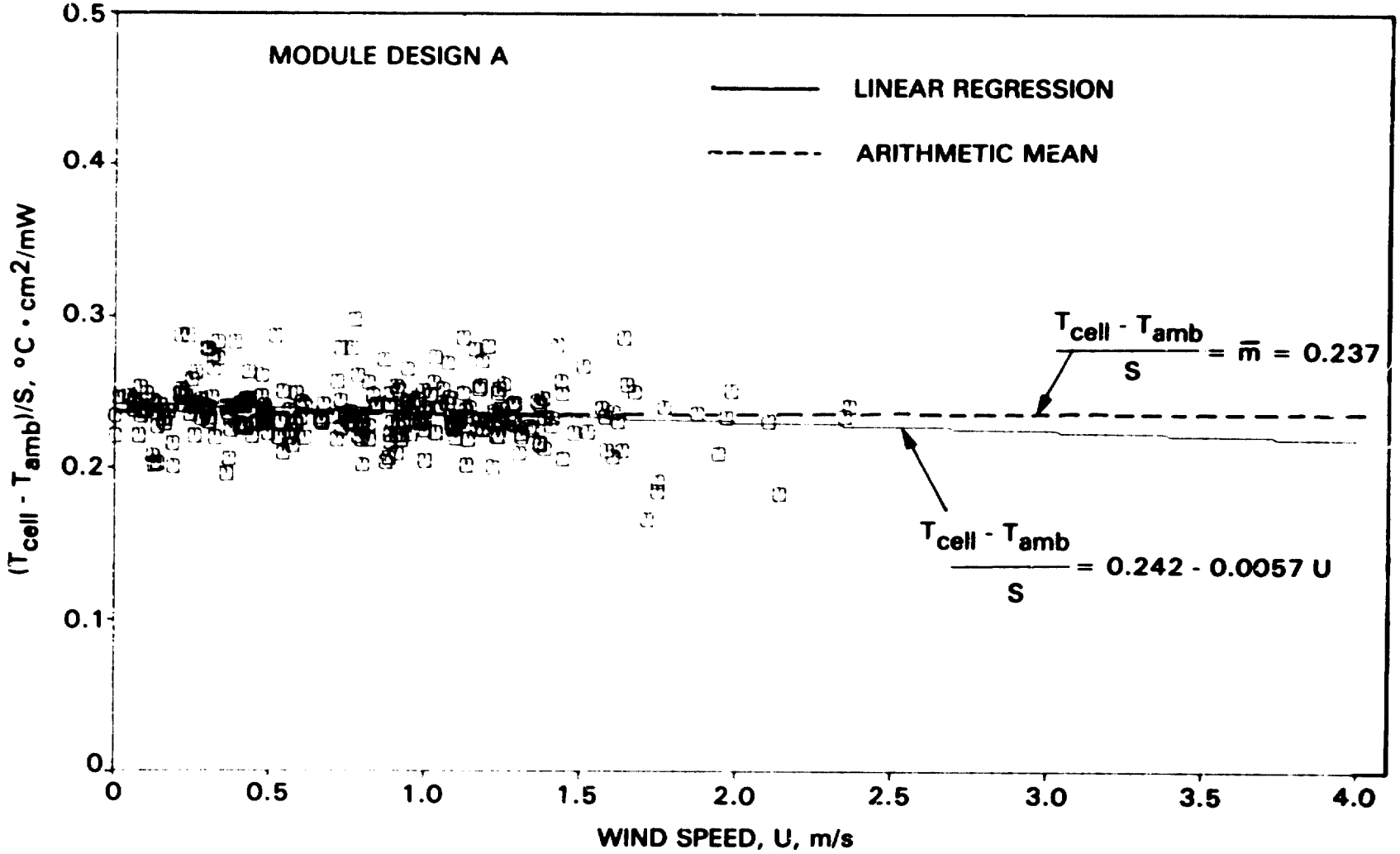

Figure 3-6. $(T_{cell}-T_{amb})/S$ versus Wind-Speed Measurements for Sensor Technology Block I Module at JPL Field-Test Site

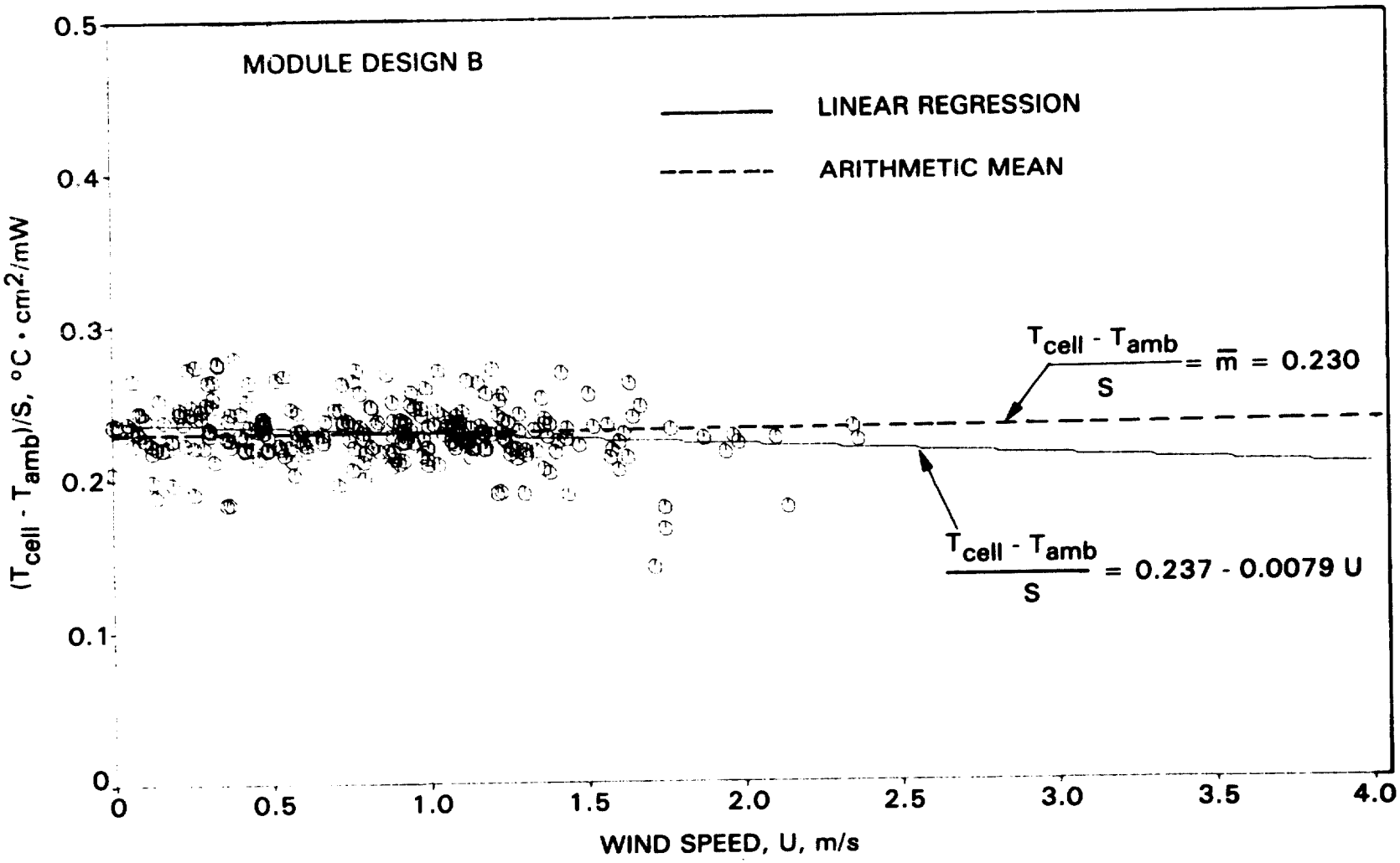

Figure 3-7. $(T_{cell}-T_{amb})/S$ versus Wind-Speed Measurements for Spectrolab Block I Module at JPL Field-Test Site

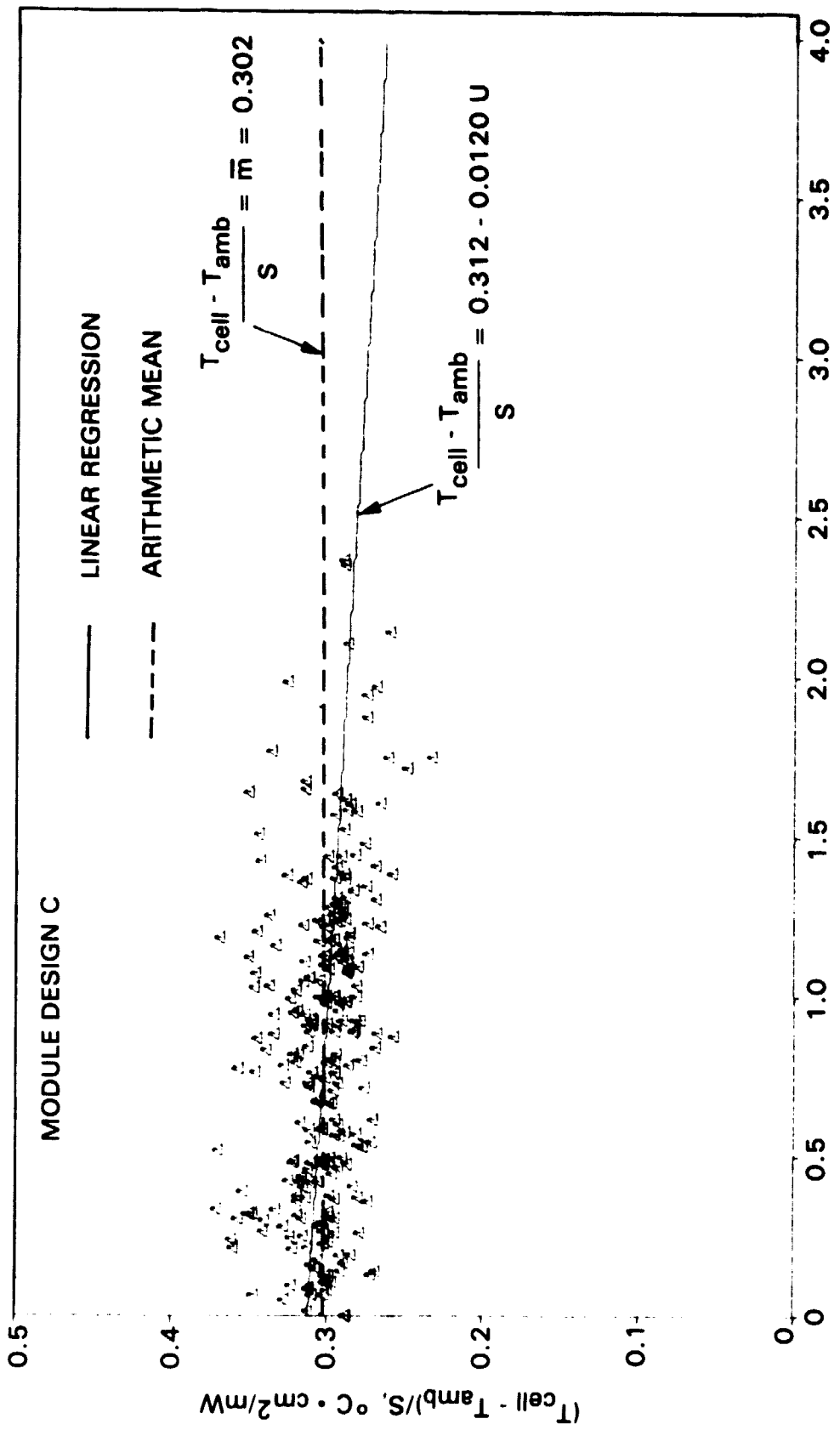

Figure 3-8. $(T_{cell}-T_{amb})/S$ versus Wind-Speed Measurements for Solarex Block I Module at JPL Field-Test Site

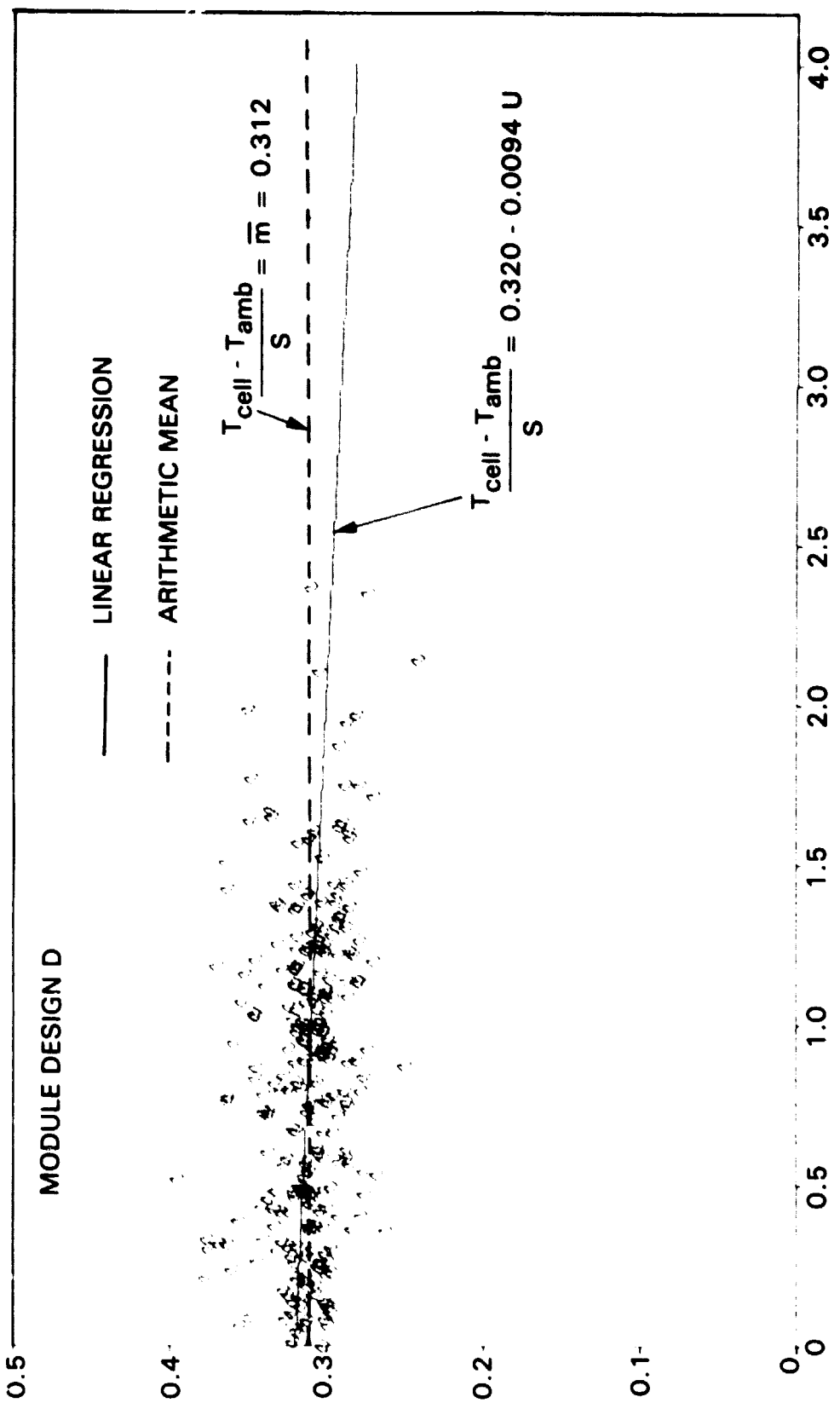

Figure 3-9. $(T_{cell}-T_{amb})/S$ versus Wind-Speed Measurements for Solar Power Block I Module at JPL Field-Test Site

roughness until the altitude reaches the gradient height, which is typically 330 m (1000 ft) or more. Above the gradient height there is no retardation of airflow because the ground surface and the wind profile would become uniform. Below this critical level, the effective wind speed can be approximated by the established relationship (References 15 and 16) shown in Equation (15) for most engineering applications.

$$\left(\frac{V_Z}{V_{30}}\right) = \left(\frac{900}{30}\right)^{1/7}\left(\frac{Z}{Z_G}\right)^{1/\beta} \tag{15}$$

where

V_Z = effective wind speed at altitude Z ft

V_{30} = reference wind speed measured at 30 ft above ground

Terrain	β	Z_G
Open	7	900 ft
Suburb	4.5	1200 ft
City	3	1500 ft

According to Equation (15), the effective wind speed near the module, V (at 1.5 m or 5 ft above ground), can be estimated from Equation (16) based upon the measured wind speed, υ (at 6 m or 19.68 ft above ground), with a terrain constant, β, of 3, and an altitude constant, Z_G, of 1500 ft.

$$\frac{V}{\upsilon} \approx \left(\frac{900}{19.68}\right)^{1/7}\left(\frac{5}{1500}\right)^{1/3} = 0.258 \tag{16}$$

It should be noted that the test conditions at the JPL test site are not time-invariant. The module tilt angle is changed every three months. This provides a relatively constant insolation level for performance measurements, but both the convective and radiative heat-transfer characteristics are altered. In addition, the topography and the environment were changed over the years by adding more module stands. Furthermore, screening of the records reveals that the maintenance of measurement equipment was less than desirable. Many sets of wind data were clearly in error, since negative wind speeds and those greater than 150 mph are not possible. Some insolation data were also questionable. Most of these doubts were found in the latter part of the record. It is possible that these were caused by equipment errors.

SECTION IV

STEADY-STATE ANALYSIS

The thermal behavior of a photovoltaic module seldom reaches steady-state conditions in a natural environment, because all of the pertinent parameters such as insolation, wind condition, and ambient temperature fluctuate with time. Nevertheless, steady-state analysis presents the simplest condition for the investigation of wind-cooling effect. In this special situation, all environmental inputs are time-invariant. The process of establishing the correlation between experimental data and analytical predictions is much more simplified.

A. SIMULATION OF CONTROLLED TESTING

Controlled testing inside the solar simulator represents a rare case of steady-state condition. The result can be used as a reference case to calibrate the analytical technique.

A detailed thermal network model of the ASEC PV module was constructed and steady-state thermal analysis was made under proper boundary conditions. The model was first calibrated with reported NOCT data. The established thermal model was then used to evaluate the forced-convection heat-transfer coefficient by matching the analytical temperature predictions with the measured data reported in Reference 13. Figure 4-1 illustrates the forced-convective heat-transfer coefficient for different wind speeds; for a fixed wind direction, the correlation is fairly linear. Figure 4-2 shows that the value of the coefficient of heat transfer is affected by wind direction, with the highest value corresponding to the range of 90 to 120 deg. It is worth noting that the integrated average value over all wind directions, assuming equal weighting for any direction, agrees well with the expression in Equation (14).

B. LINEARIZED APPROXIMATION

A detailed thermal network model of a system consists of many lumped-mass nodes, and the energy Equation (5) has many non-linear terms. However, the relationship can be greatly simplified if the following assumptions are made:

(1) Free-convective heat transfer can be linearized and represented by an average coefficient of heat transfer, h.

(2) Radiative heat transfer can also be linearized by an effective radiative conductance coefficient, h_r.

(3) Temperature gradient along the module is ignored. Heat loss conducted through the module, Q_{cond}, can be approximated by Equation (17):

$$Q_{cond} = (T_{cell} - T_S) \frac{KA}{L} \qquad (17)$$

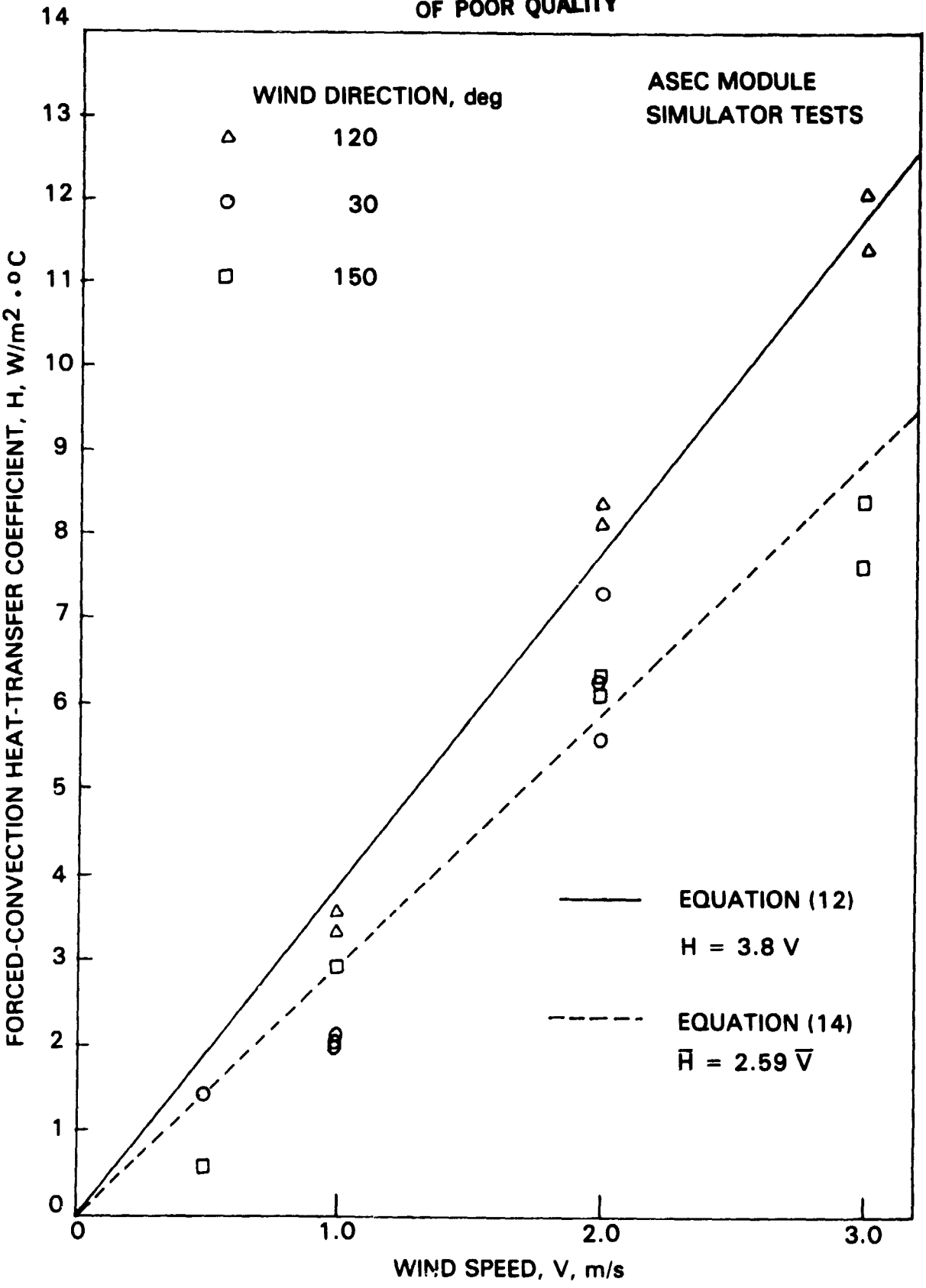

Figure 4-1. Forced-Convection Heat-Transfer Coefficient versus Wind Speed

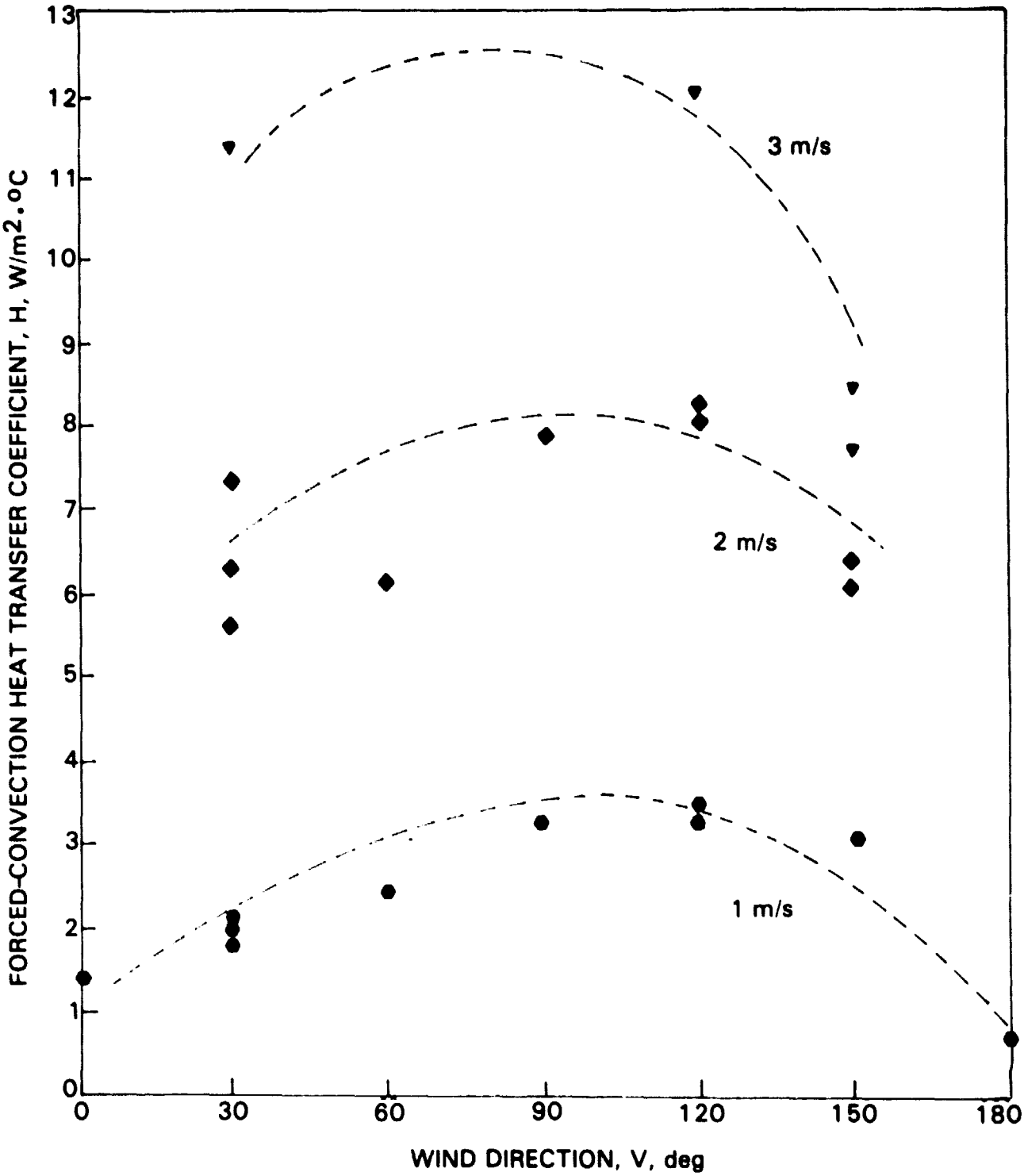

Figure 4-2. Forced-Convection Heat-Transfer Coefficient versus Wind Direction

where

T_{cell} = cell temperature

T_S = surface temperature

K = effective conductivity

L = effective thickness

The linearized energy Equation (5) can be reduced to the following for a steady-state condition:

$$T_{cell} - T_{amb} = \frac{\alpha^*}{C} \cdot S \tag{18}$$

where

C = effective unit heat-transfer conductance
α^* = pseudo-effective solar conductance coeffected for power extraction, P

$$\alpha^* = \alpha - \frac{P}{AS} \tag{19}$$

$$\frac{1}{C} = \frac{1}{(h + h_r + H)_{front} + (h + h_r + H)_{back}} + \frac{L}{K} \tag{20}$$

It is clear that the value of effective conductance, C, is a function of ambient temperature, wind condition, and module thermal design. To establish a relative basis for comparison, one may define a reference conductance, C_o, that is consistent with NTE.

$$T_{cell} - T_{amb} = \frac{C_o}{C} \cdot m_o \cdot S \tag{21}$$

where m_o is the sensitivity constant for a reference condition of 1 m/s wind speed, and 20°C ambient temperature. The normalized conductance ratio, C_o/C, characterizes the dependency on environmental parameters (i.e., wind speed and ambient temperature). C_o/C can be evaluated based upon the established thermal models for various module designs. Figure 4-3 shows the variation of C_o/C for different levels of effective wind speed, $\bar{V}$. It can be seen that the relationships for module designs C and D (Solarex and Solar Power) are very close because their design configurations are very similar. However, module designs A and B (Sensor Technology and Spectrolab) display different sensitivity relationships, because the designs have different fin structures on the module back surfaces. The relationship between C_o/C and ambient temperature level is shown in Figure 4-4. The difference in module thermal designs does not seem to affect this sensitivity relationship.

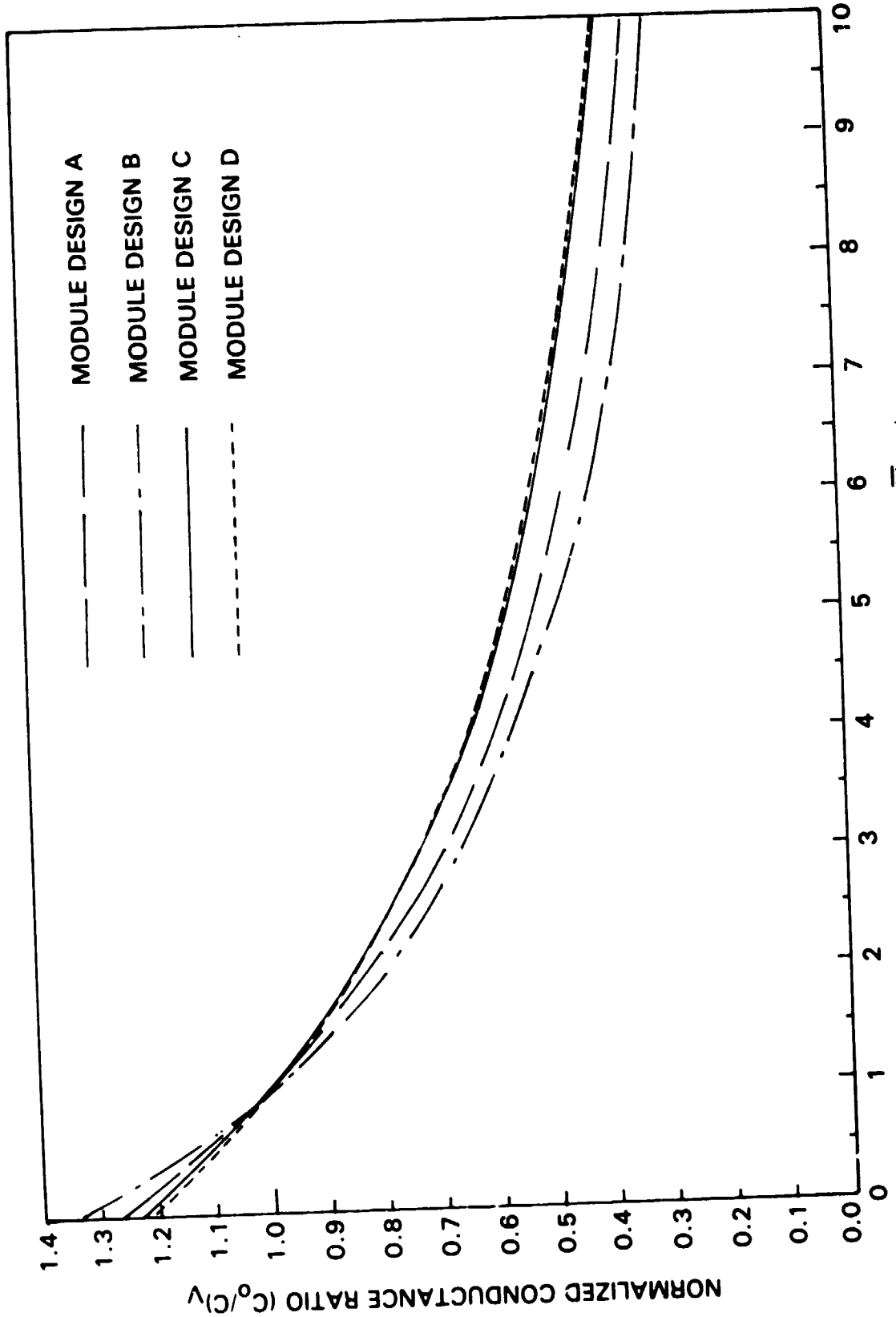

Figure 4-3. Effect of Wind Speed on Normalized Conductance Ratio

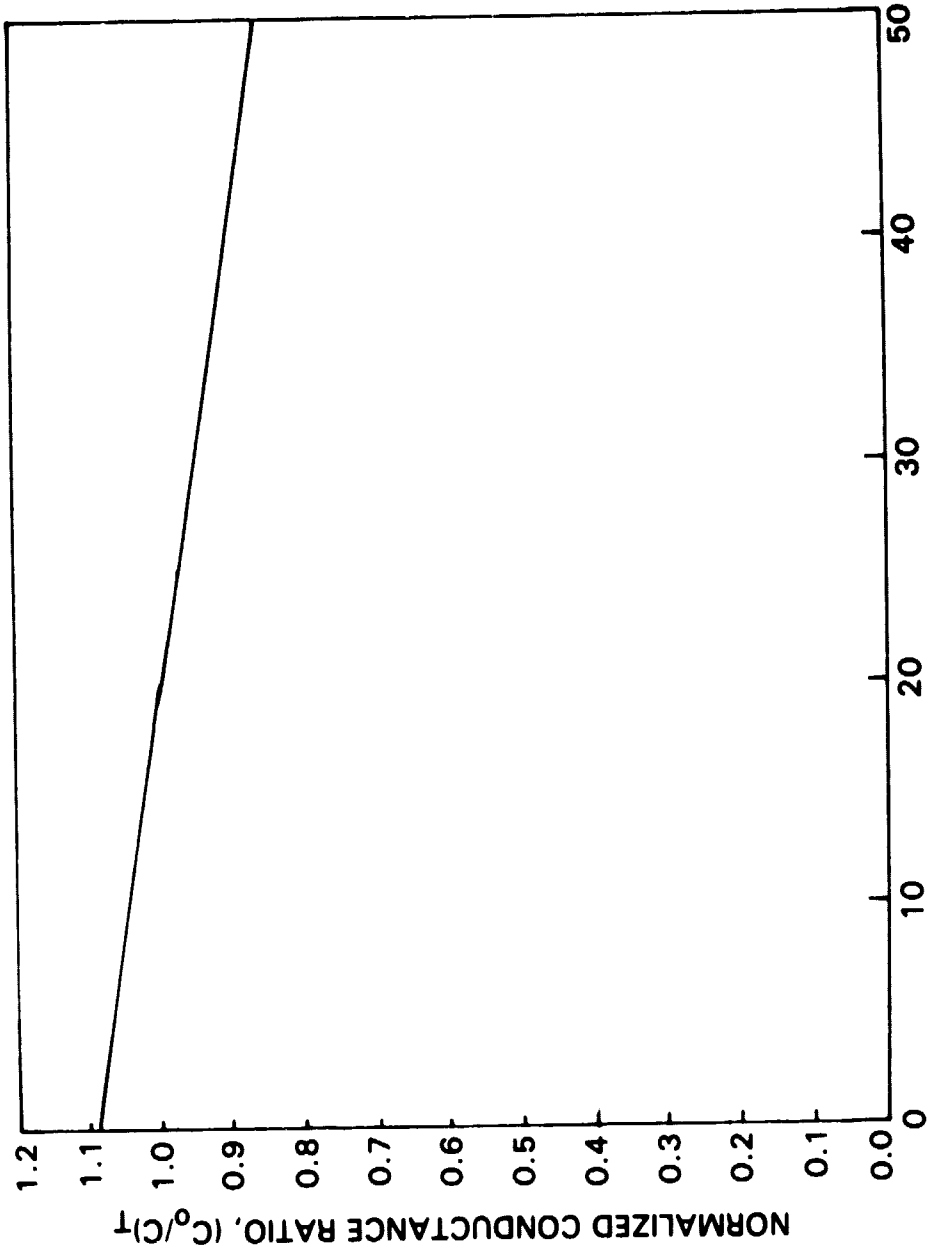

Figure 4-4. Effect of Ambient Temperature on Normalized Conductance Ratio

The relationships shown here can be used to assess steady-state module temperature. For example, the reference sensitivity constant, m_o, for module design C is 0.302 at 1 m/s, 20°C. The estimated cell temperature at 35°C ambient ($C_o/C = 0.927$), 2 m/s wind ($C_o/C = 0.85$), and 95 mW/cm^2 insolation can be evaluated from

$$(T_{cell} - T_{amb}) = \left(\frac{C_o}{C}\right)_T \cdot \left(\frac{C_o}{C}\right)_{\bar{V}} \cdot m_o \cdot S \qquad (22)$$

or

$$T_{cell} = 35^{\circ}C + 0.927 \times 0.85 \times 0.302 \times 95$$

$$= 57.6^{\circ}C$$

SECTION V

PSUEDO-STEADY-STATE APPROXIMATION

A. TRANSIENT THERMAL RESPONSE

The thermal behavior of a photovoltaic module rarely reaches a steady-state condition in a natural environment. This is because of the changing environmental parameters: insolation, ambient temperature, and wind. The module temperature at any specific time is not just a function of the instantaneous environmental parameter values, but rather is a function of the time-varying process governed by the energy balance, initial temperature, and pertinent boundary conditions.

In a linearized form, the energy Equation (5) can be written as follows:

$$\frac{MC_p}{A}\frac{dT}{dt} = \alpha^* \cdot S - C\left(T - T_{amb}\right) \tag{23}$$

The values of insolation, S, and ambient temperature, T_{amb}, vary with time. The unit conductance, C, is a function of wind, which fluctuates with time.

One of the major drawbacks of transient analysis is the lack of available thermal and environmental data. Most of the weather records, such as the SOLMET tape, represent a sampling of instantaneous values taken every hour or every 15 min. Module temperature measurement data are even harder to obtain. The JPL field-test data indicating module temperatures are recorded only once every 24 h. Therefore, a transient thermal analysis cannot be performed accurately with the available data.

B. TRANSFER FUNCTIONS

Because transient analysis is too complex and a steady-state solution does not include time variations, it is difficult to correlate experimental results in natural environments. A concept of transfer function is proposed here, as a practical approximation, to include the time variations of environmental parameters, so that module thermal response can be treated in a simple linear relationship. The procedure for transfer function calculations involves a detailed transient analysis of module thermal response. A multi-node thermal model of a specific module design was first constructed and the thermal response under a reference environment is computed. In this reference case the environmental parameters, such as insolation, S, ambient temperature, T_{amb}, and effective wind speed, were assumed to be constant and the resultant module temperature is T^o. In a series of perturbation calculations, each parameter is simulated by a pulse of changes at different time instances, t. The corresponding transfer function is calculated as the equivalent change in the parameter in a steady-state manner.

In order to illustrate the procedures for determining transfer functions, a sample calculation of $\Phi_T(\tau)$ (transfer function for ambient temperature change) is shown as follows:

(1) Let us consider that the NOCT of a specific module is 45°C. (i.e., the steady-state temperature T^o under NTE).

(2) These NTE parameters are maintained at constant levels of 80 mW/cm^2, 20°C and 1 m/s wind, except that the ambient temperature was increased +10°C (to 30°C) for 1 min at time (t - 15 min), before returning to the reference temperature of 20°C. The corresponding module temperature at t is observed to be 45.5°C.

(3) A steady-state module temperature of 45.5°C under 80 mW/cm^2 and 1 m/s environment corresponds to an ambient temperature of 20.5°C.

It can be seen that for this specific module a change in ambient temperature of 10°C for 1-min duration, 15 min before the measurement time would be equivalent to a change of 0.5°C in the psuedo-steady-state ambient temperature. Therefore, in other words, the transfer function Φ_T (15 min) is 0.05.

After all the transfer functions are evaluated for different time instances, pseudo-steady-state quantities can be assessed for ambient temperature, insolation and wind speed according to Equations (24) to (26).

$$T^*_{amb} = T^o_{amb} + \frac{\int_{t-\Delta t}^{t} \left[T_{amb}(\tau) - T^o_{amb}\right] \phi_T(\tau) d\tau}{\int_{t-\Delta t}^{t} \phi_T(\tau) d\tau} \tag{24}$$

$$S^* = S^o + \frac{\int_{t-\Delta t}^{t} \left[S(\tau) - S^o\right] \phi_S(\tau) d\tau}{\int_{t-\Delta t}^{t} \phi_S(\tau) d\tau} \tag{25}$$

$$\bar{V}^* = \bar{V}^o + \frac{\int_{t-\Delta t}^{t} \left[\bar{V}(\tau) - \bar{V}^o\right] \phi_V(\tau) d\tau}{\int_{t-\Delta t}^{t} \phi_V(\tau) d\tau} \tag{26}$$

Once these pseudo-steady-state environmental variables are evaluated based upon the time series of variations, the module temperature at time t can be expressed as

$$C^* \left(T_{cell} - T^*_{amb}\right) = \alpha^* S^* \tag{27}$$

Figures 5-1 through 5-3 show the computed transfer functions of the four module designs. The transfer functions for insolation, ϕ_S, for ambient temperature, ϕ_T, and for effective wind speed, ϕ_V, are very similar for a specific module design. For all practical purposes, they can all be represented by a single function, $\phi(\tau - t)$, which is a function of the module thermal inertia and time. Module designs A and C have similar thermal inertia per unit area, while module designs B and D have close values as shown in Table 2-1. For module designs of light thermal inertia, such as module design C, the thermal response is more sensitive to the instantaneous environmental changes and is less sensitive to the variations in the past.

C. PSEUDO-STEADY-STATE ANALYSIS OF FIELD-TEST DATA

Field-test measurements obtained at the JPL test site were correlated in this report to demonstrate the proposed pseudo-steady-state approximation technique. Because of the change in the module mounting configuration and measurement uncertainties, only the data set obtained in the period of June through August 1978 was used. The sampling frequency for environmental parameters was 15 min. Variations in insolation level and ambient temperature were interpolated between data points. The concept of transfer functions was applied to obtain the pseudo-steady-state quantities, S^* and T^*_{amb}. The sampling frequency was considered to be too slow to provide meaningful resolution for wind-speed variations; therefore, no meaningful pseudo-steady- state wind, V^*, can be computed. Instead, an average effective wind speed, $V^\#$, adjusted according to Equation (16), was used in characterizing the effective wind conditions.

Figures 5-4 through 5-7 show the average effective unit conductance, per surface, $C^*/2$, evaluated using Equation (27). The values were plotted versus the corresponding average effective wind speed, $V^\#$. The data can be curve fitted with a least squares linear regression expression of $C^*/2 = a + b \cdot V^\#$. The coefficient, a, is the heat-transfer coefficient for free convection and thermal radiation. The value ranges from 9.07 and 10.25 $W/m^2 \cdot {}^oC$ for module designs C and D, to 11.67 $W/m^2 \cdot {}^oC$ for module A and 12.66 $W/m^2 \cdot {}^oC$ for module design B. Module designs A and B have design fins on the rear surfaces to increase the heat-transfer rate to the ambient. The sensitivity coefficient, b, is evaluated to be 2.37 and 2.71 $W/m^2 \cdot {}^oC/(m/s)$ for module designs C and D. The values for module designs A and B are 1.86 and 2.07, respectively. These values appear to be in general agreement with the effective value of 2.59 $W/m^2 \cdot {}^oC/(m/s)$ shown in Equation (14).

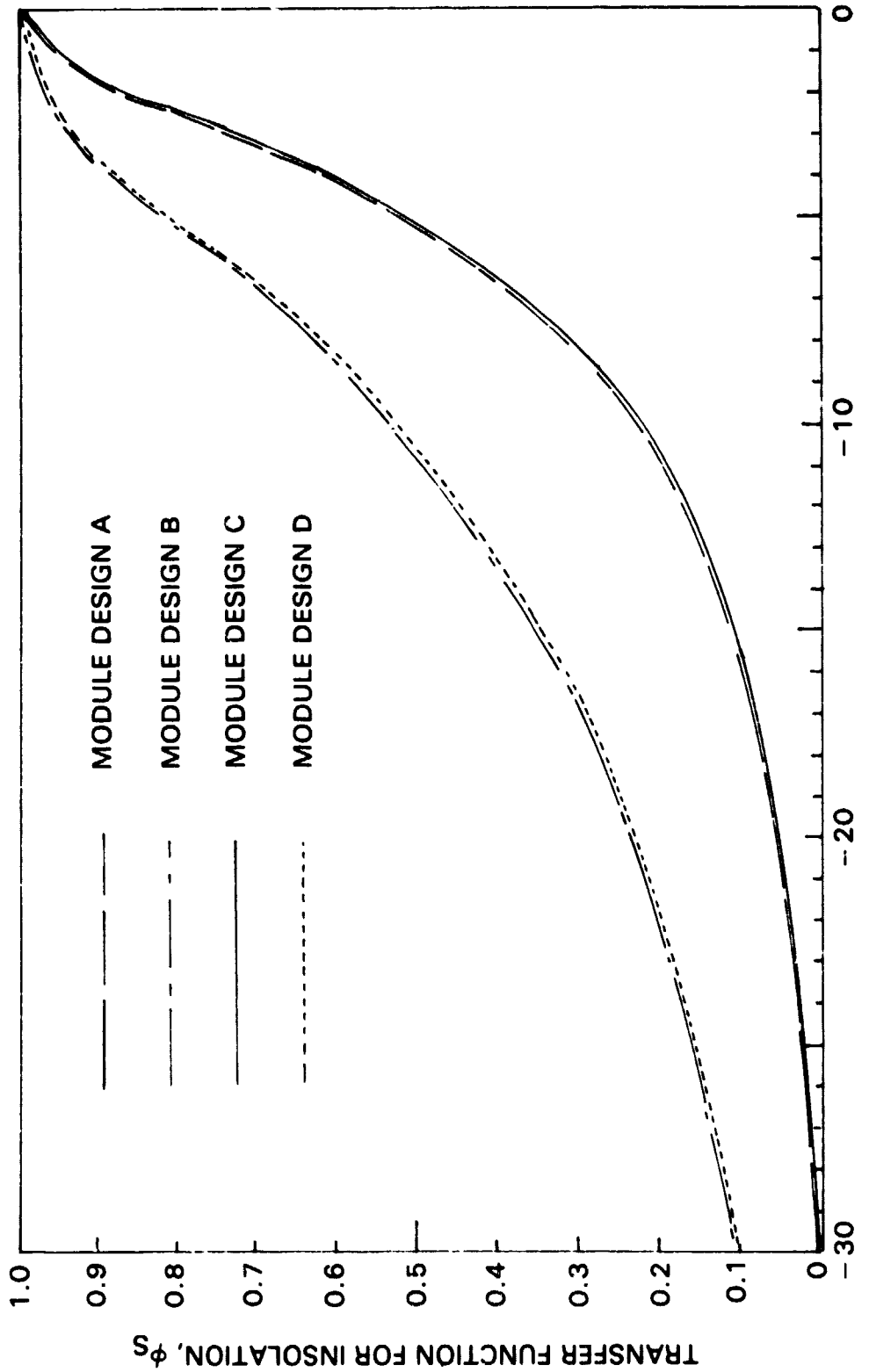

Figure 5-1. Transfer Functions for Instantaneous Insolation Values

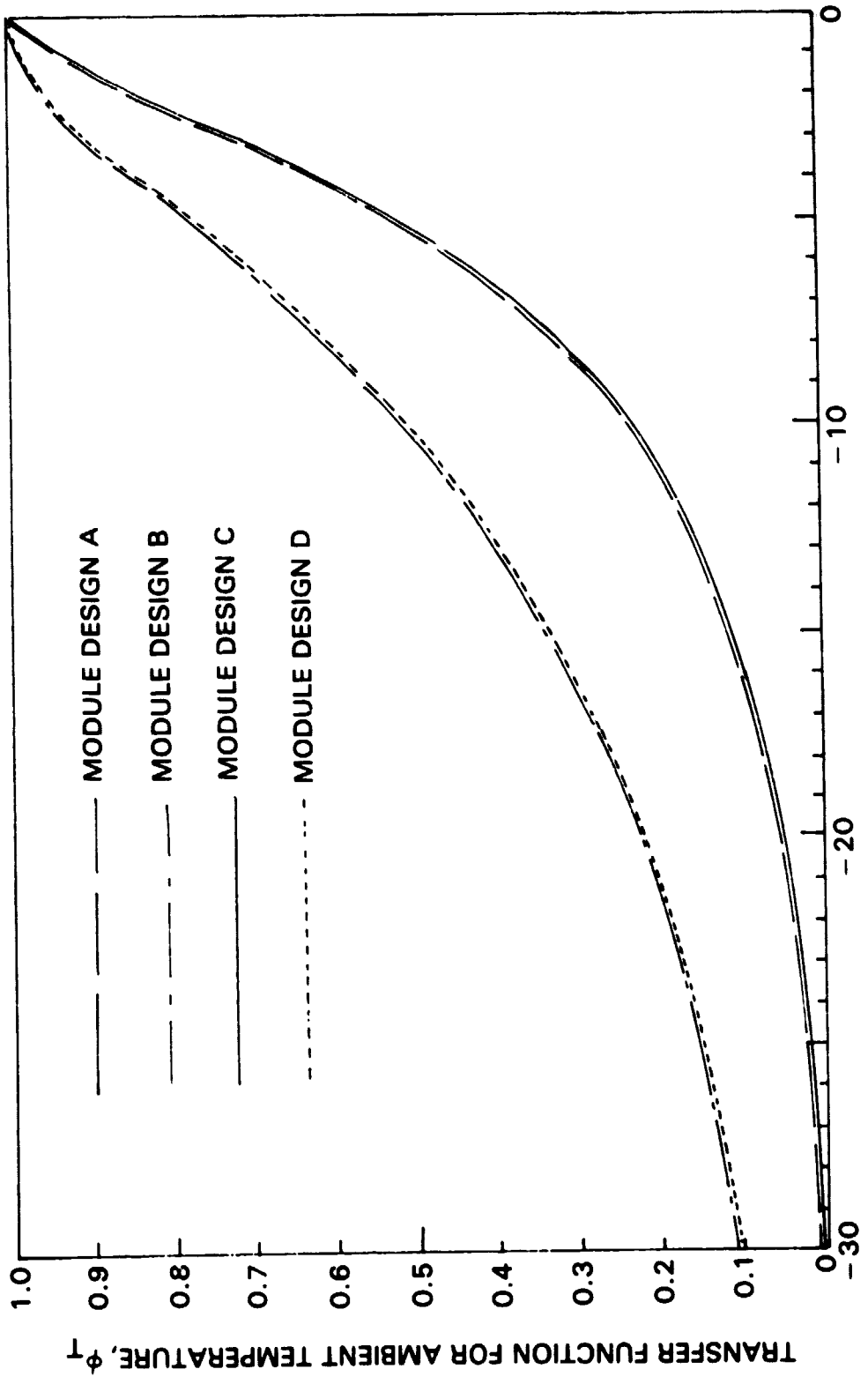

Figure 5-2. Transfer Functions for Ambient Temperature

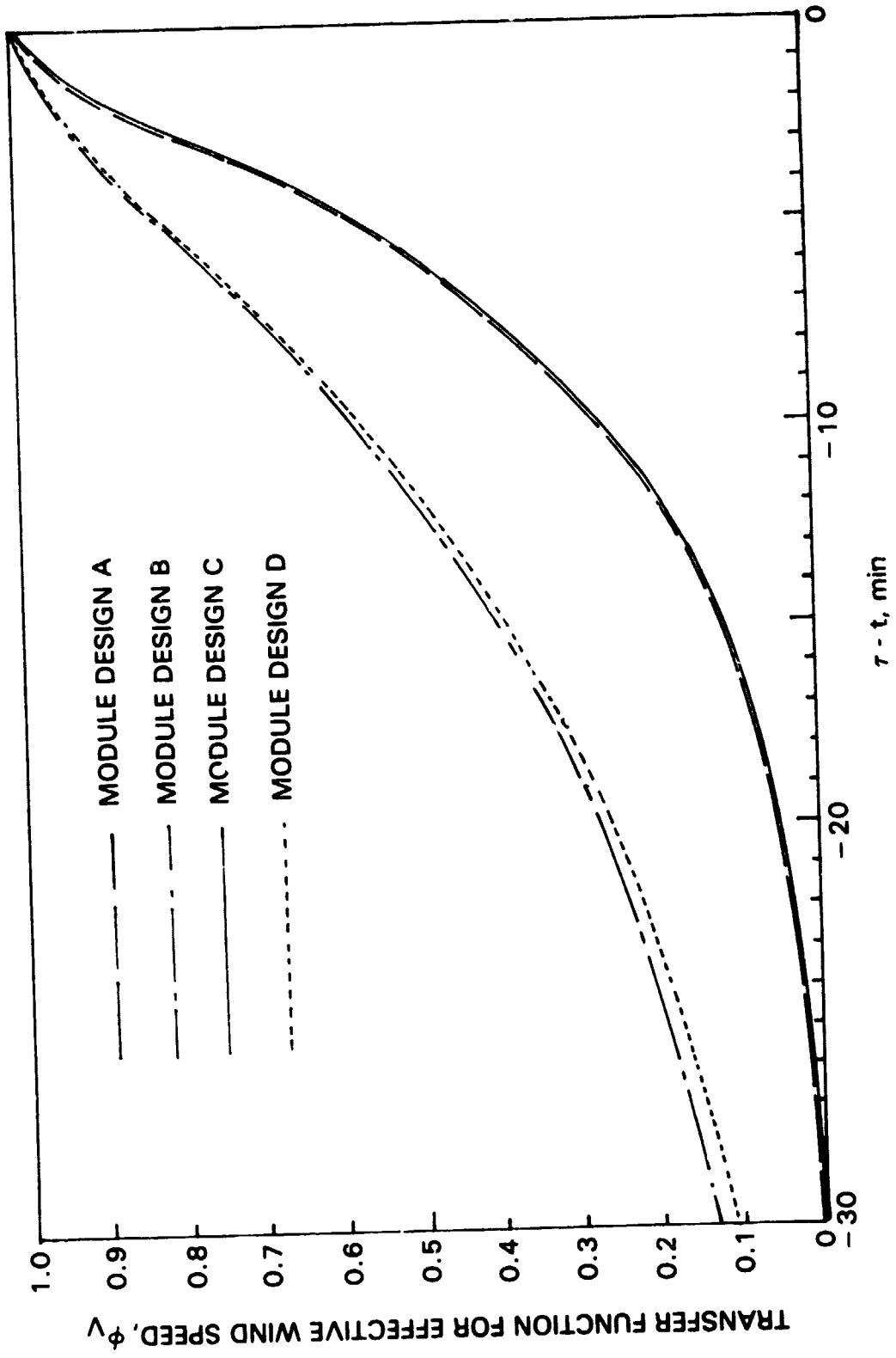

Figure 5-3. Transfer Functions for Effective Wind Speed

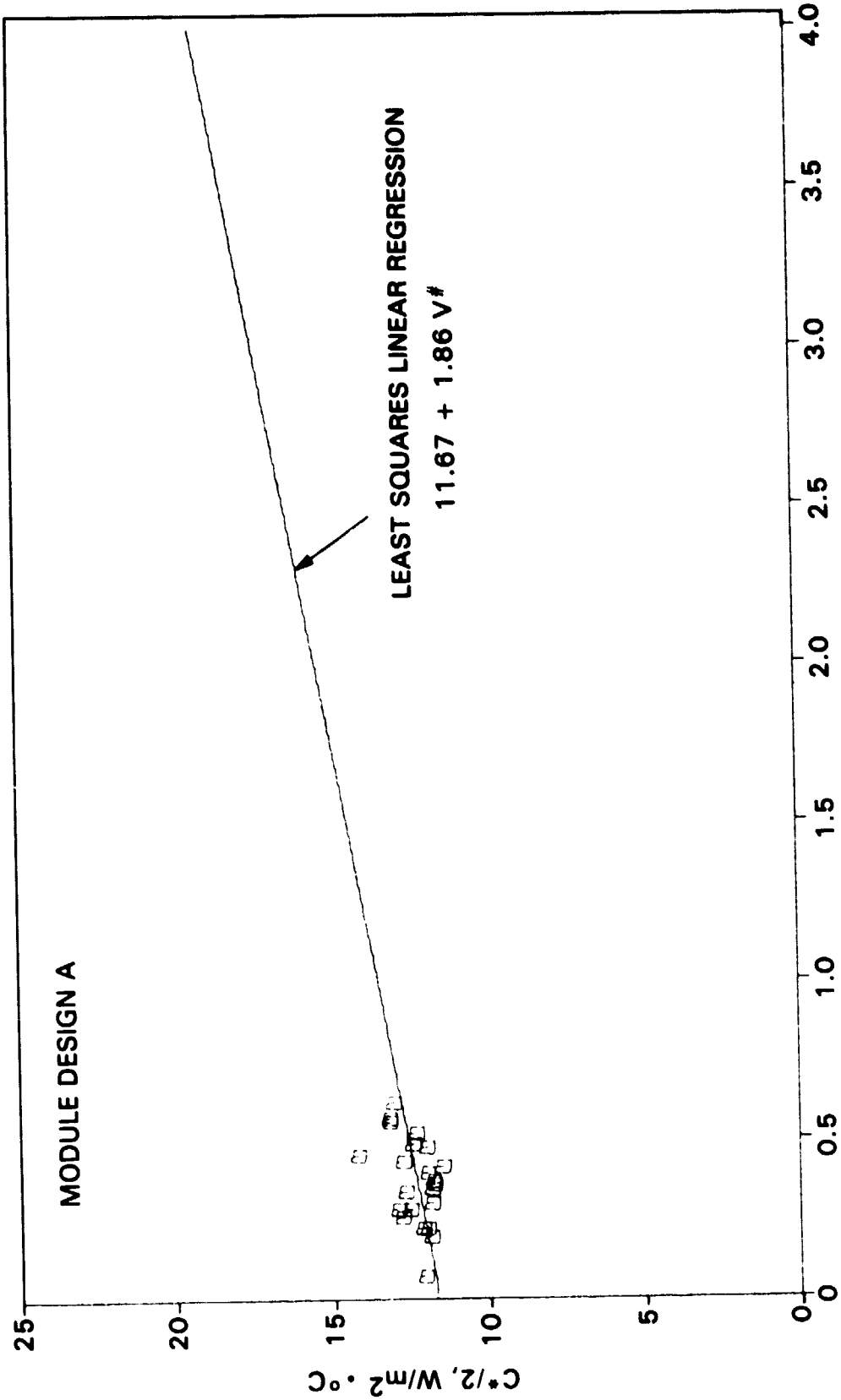

Figure 5-4. Unit Conductance versus Wind Speed for Sensor Technology Block I Module

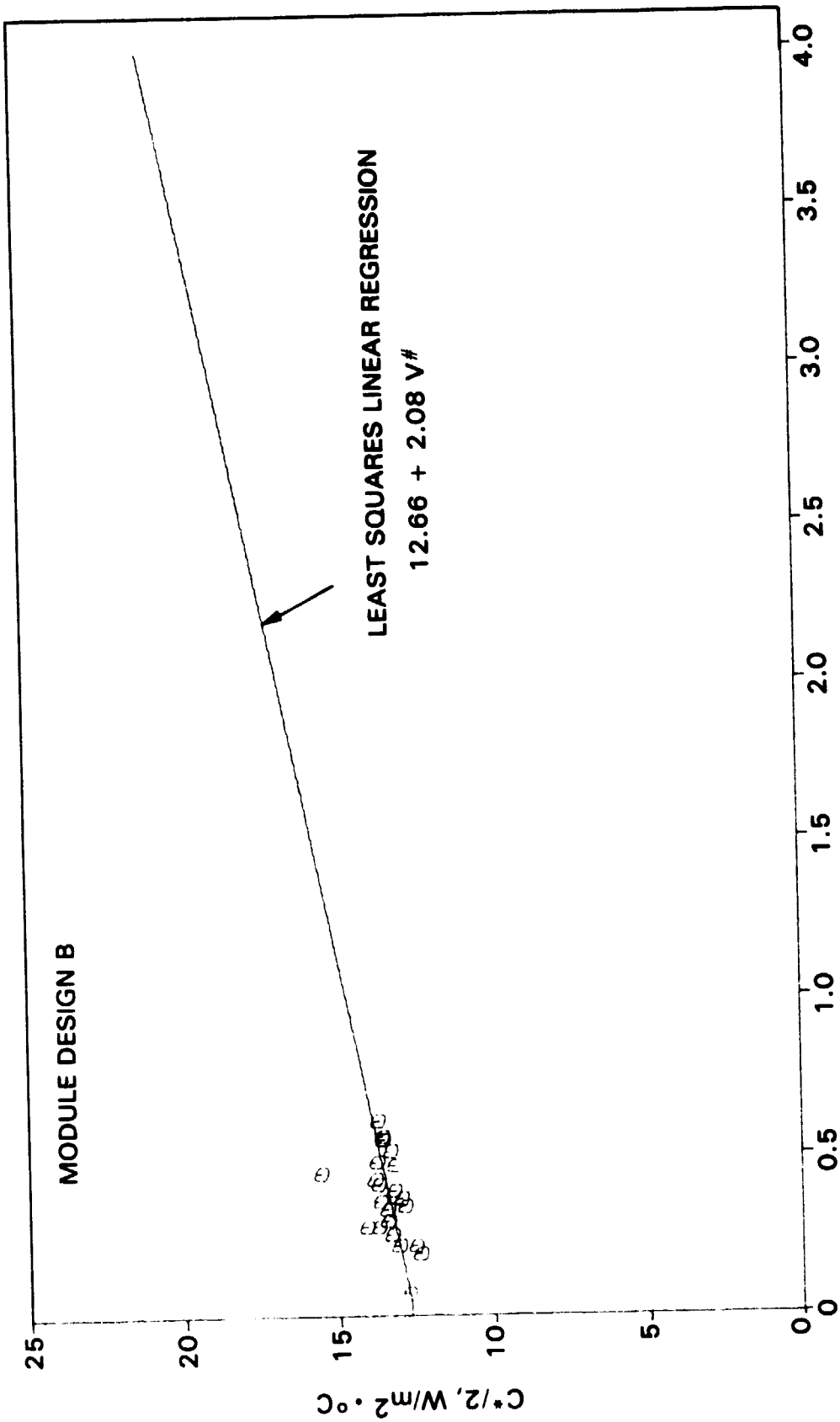

Figure 5-5. Unit Conductance versus Wind Speed for Spectrolab Block I Module

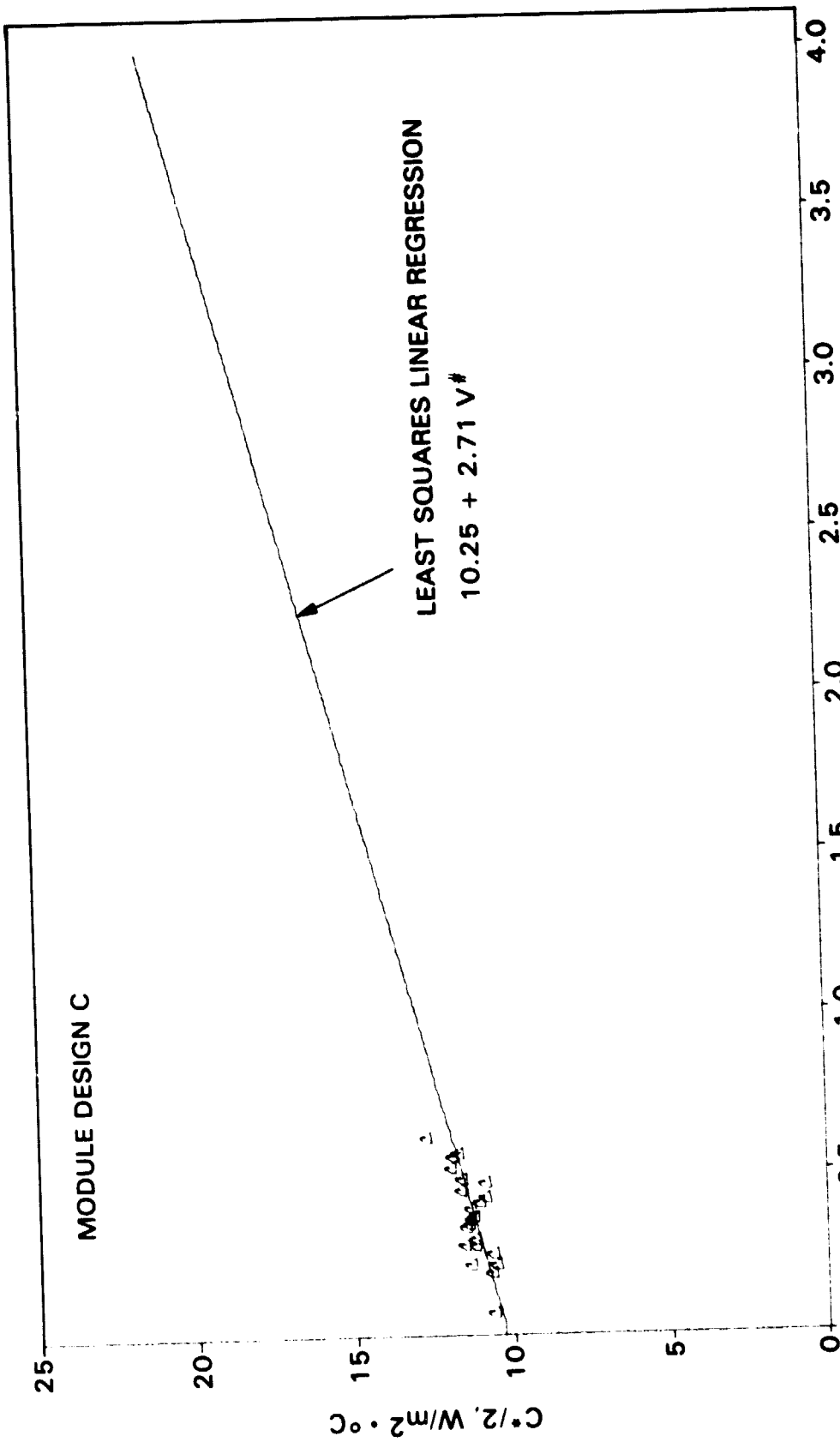

Figure 5-6. Unit Conductance versus Wind Speed for Solarex Block I Module

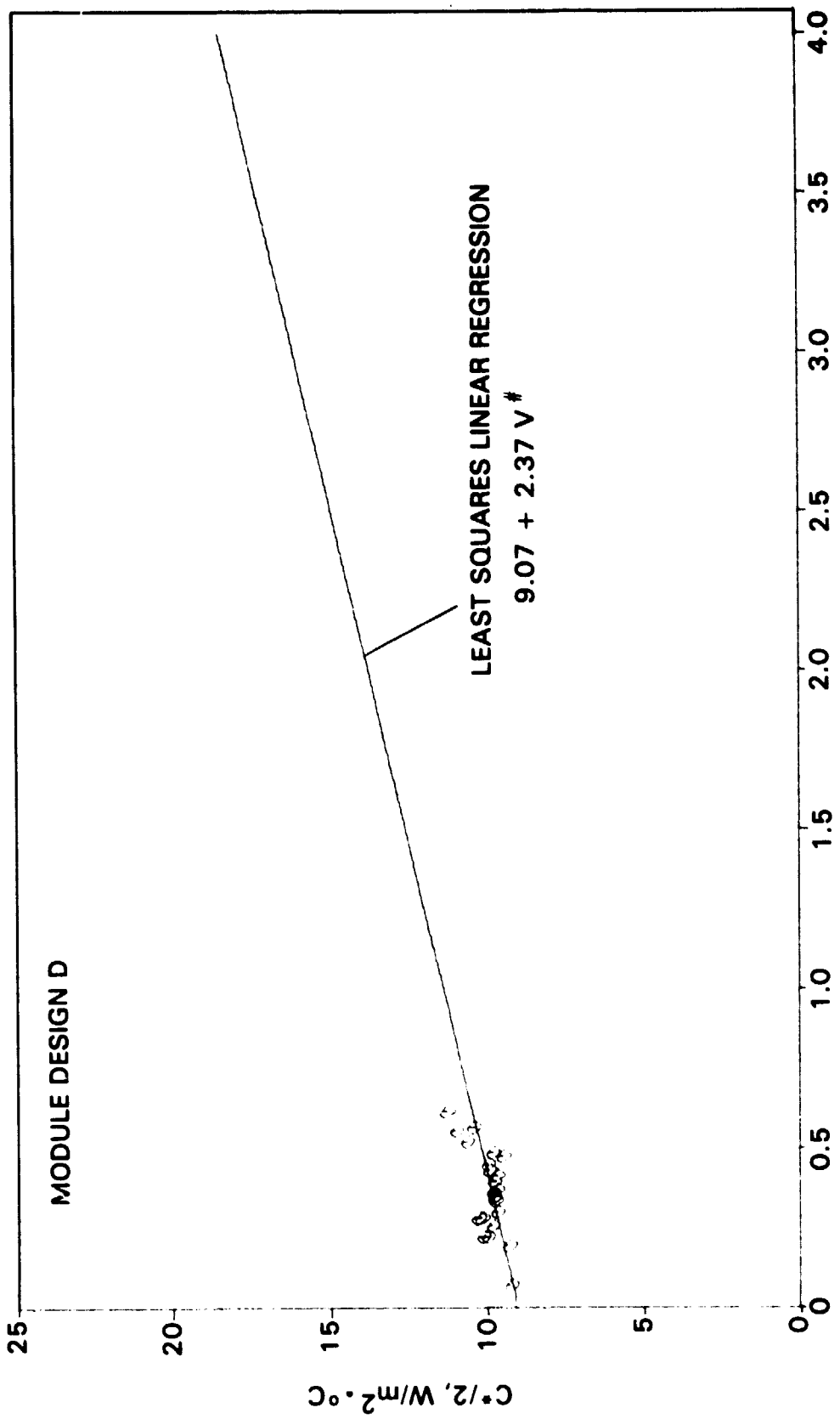

Figure 5-7. Unit Conductance versus Wind Speed for Solar Power Block I Module

SECTION VI

CONCLUSIONS

The effect of wind cooling on photovoltaic arrays is governed by wind speed, wind direction, and the location of wind measurement. For unidirectional wind parallel to module surfaces, the cooling effect can be expressed by the established convective heat-transfer correlation: $H = 3.8\ V$. Experimental data obtained in controlled chamber tests confirm this correlation.

The cooling by natural wind can be approximated by an average coefficient of convective heat transfer, $\bar{H}$, which can be correlated linearly with the effective wind speed averaged in all directions. The relationship, $\bar{H} = 2.59\ \bar{V}$, which agrees with the observation in the chamber test, is recommended for predicting PV module thermal performance in a field. Wind measurement location appears to be the critical factor that determines the validity of the correlation between convective heat transfer and wind speed. Wind condition measurements at weather stations or test sites are typically taken at a height different from the module level. The effective wind speed for module convective cooling should be measured at the average module height and could be significantly less than that measured at higher altitude. Power-law relationship has been established to relate wind speeds at different altitudes. Applying this power-law profile on field-test data obtained at the JPL test site resulted in reasonably good agreement between the test results and the established heat-transfer correlation. It should be cautioned, however, that limited test data were analyzed. Furthermore, the range of measured wind-speed variation was very limited; the maximum wind-speed variation, after scaled down from a height of 6 m to 1.5 m (the ratio of wind-speed retardation is about 4:1), would be around 0.6 m/s. As a result, the experimental uncertainty level is larger than the signal to be detected. In other words, although the field-test experimental data show general agreement with the established correlation, nevertheless, the data do not cover sufficient range and should not be viewed as conclusive. Direct-wind data comparisons between weather-station recording and in-situ wind measurements near the module should be made in future experiments to establish a reliable method for assessing the effective wind speed.

SECTION VII

REFERENCES

1. Ross, R. G., and Gonzalez, C. C., "Reference Conditions for Reporting Terrestrial Photovoltaic Performance," a paper presented at the AS/ISES 1980 Annual Meeting, Phoenix, Arizona, June 2-6, 1980.

2. Gonzalez, C. C., and Ross, R. G., "Performance Measurement Reference Conditions for Terrestrial Photovoltaics," a paper presented at the AS/ISES 1980 Annual Meeting, Phoenix, Arizona, June 2-6, 1980.

3. Stultz, J. W., Thermal and Other Tests of Photovoltaic Modules Performed in Natural Sunlight, JPL Internal Report No. 5101-76, DOE/JPL-1012-78/9, Jet Propulsion Laboratory, Pasadena, California, July 31, 1978.

4. Barstow Insolation and Meteorological Data Base, Report No. ATR-78 (7695-05)-2, Aerospace Corporation, El Segundo, California, March 1978.

5. Feasibility Study of Solar Dome Encapsulation of Photovoltaic Arrays, Phase 1 Final Report, DOE/JPL 954833-78/1, Boeing Engineering and Construction, Seattle, Washington, December 1978.

6. Ware, J. C., "Clear Sky Temperature," a paper presented at ISES Meeting, Fort Collins, Colorado, August 1974.

7. Raithby, G. D., and Hollands, H. G. T., "A General Method of Obtaining Approximate Solutions to Lamnar and Turbulent Free-Convection Problems," Advances in Heat Transfer, Vol. II, pp. 265-315, Edited by T. F. Irvine and J. P. Hartnett, Academic Press, 1975.

8. Duffie, J. A., and Beckman, W. A., Solar Energy Thermal Processes, John Wiley and Sons, 1974.

9. McAdams, W. H., Heat Transmission, 3rd Edition, McGraw-Hill Book Co., Inc., New York, 1954.

10. Stultz, J. W., and Wen, L., Thermal Performance Testing and Analysis of Photovoltaic Modules in Natural Sunlight, JPL Internal Report No. 5101-31, Jet Propulsion Laboratory, Pasadena, California, July 29, 1981.

11. Jaffe, P., LSA Field Test Annual Report, August 1977-August 1978, JPL Internal Report No. 5101-85, DOE/JPL-1012-78/12, Jet Propulsion Laboratory, Pasadena, California, September 15, 1978.

12. Third Generation Design Solar Cell Module LSA Task V, Large-Scale Production, DOE/JPL-955409-80/1, Applied Solar Energy Corp., City of Industry, California, August 1980.

13. Griffith, J. S., Rathod, M. S., and Paslaski, J., "Some Tests of Flat Plate Photovoltaic Module Cell Temperatures in Simulated Field Conditions," a paper presented at 15th IEEE Photovoltaic Specialists Conference, Kissimmee, Florida, May 12-15, 1981.

14. Garstang, M., Snow, J. W., and Emmitt, G. D., "Wind Shear and Gustiness at the Mod-1 Site, Boone, North Carolina," Journal of Energy, Vol. 5, No. 3, pp. 146-151, May-June 1981.

15. "Lecture Notes for Designing for Wind," Institute for Disaster Research, Texas Tech University, Lubbock, Texas, August 1-3, 1977.

16. American National Standard-Building Code Requirements for Minimum Design Loads in Buildings and Other Structures, ANSI-A58.1-1972, National Bureau of Standards, Washington, D.C., 1972.